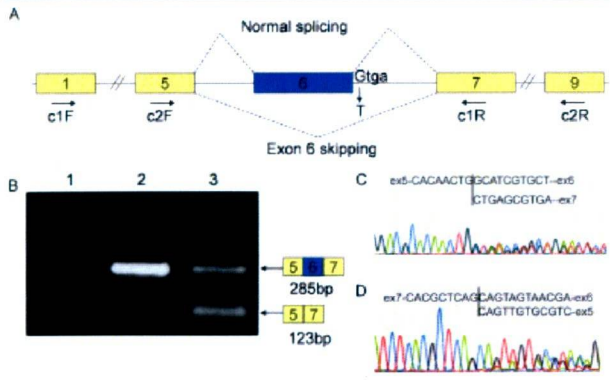

Figure 2. Skipping of exon 6 in *ACTA2* transcript due to genomic mutation in splicing donor site (c.616+1G>T) identified in Family 2. **A:** Schematic diagram of *ACTA2* normal splicing and skipping of exon 6 caused by a mutation in the splice donor site of intron 6. Positions of the primers used for RT-PCR analysis are indicated by arrows. **B:** RT-PCR analysis of *ACTA2* transcripts of the patients. cDNA samples from each patient were amplified with PCR using primers c2F and c1R, as described in (A). Exon 6 skipping and inclusion were assayed using samples from a healthy control (lane 2) and the patient (lane 3). Lane 1 shows a non-reverse-transcribed RNA control. **C,D:** Direct DNA sequence analysis of an RT-PCR fragment (c1F–c2R) representing chimeric cDNA from normal and shorter transcripts. Sequence analysis of both strands confirmed that the shorter transcript was lacking entire exon 6 (162 bp).

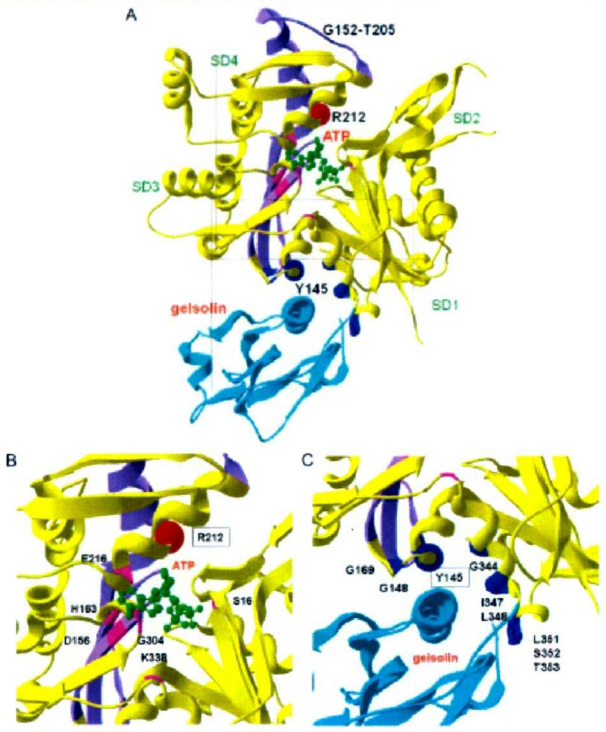

Figure 3. Estimated protein structure and mutations of ACTA2. **A:** ACTA2 monomer domain structure and associated molecules. ATP (shown in green) binding amino acids are shown in pink and gelsolin (shown in light blue) binding amino acids are shown in blue. Locations of the ACTA2 mutations are also mapped. Red and blue spheres represent R212 and Y145, respectively. Amino acids deleted by exon 6 skipping are shown in purple. **B:** Details regarding ATP binding cleft. **C:** Details regarding gelsolin binding interface.

Table S1). The six members had four Stanford A–type aortic dissections, three Stanford B–type aortic dissections, and one undefined type. Since some of the affected individuals were deceased and other family members with or without aortic diseases did not give consent, a genomic DNA sample for genetic analysis was available only from the proband.

The clinical features of this patient were unremarkable, except for early onset of aortic dissection. Although not all members could be closely examined, no ocular, skin, or cardiac abnormalities were noted in any of the remaining individuals.

Family 3

We identified a heterozygous G to A transition at cDNA position 635 in three affected members in Family 3. This mutation is located in exon 6 and predicts an amino acid substitution of Arg212 to Gln. The mutation was not found in the rest of the cohort or in 190 control subjects. Although genetic analysis was performed for three affected members (Patients III:8, IV:5, and IV:7) and three unaffected members (Patients II:3, IV:3, and IV:4), the pedigree chart suggested that the other four affected members (Patients II:1, II:4, III:2, and III:3) would be obligate carriers of this mutation. No mutation was found in any of nonaffected members tested. Arg212 is a highly-conserved amino acid in actin families located in subdomain 4 (Fig. 3B), which faces the ATP binding cleft in the crystallized protein structure and is positioned adjacent to Glu216, one of the known ATP binding sites. Arg212 has also been shown to stabilize the water-mediated hydrogen bonding network across the ATP-binding cleft [Vorobiev et al., 2003]. A substitution of basic Arg212 with a guanidinium side chain to neutral Glu, a side-chain-amide group amino acid, would disturb this stabilization and is expected to be deleterious. We also employed polymorphism phenotyping (PolyPhen) analysis [Ramensky et al., 2002] to predict the impact of the p.R212Q amino acid substitution. The algorithm predicted the substitution would be "probably damaging" because of "disruption of the ligand binding site," with a position-specific independent count (PSIC) score of 2.394 in 496 observations (>2.0 indicated "probably damaging").

The proband (Patient IV-5, index) was a 29-year-old male who was diagnosed with chronic aortic dissection (Stanford B type) at age 25 years, which was followed by a graft replacement of the descending aorta. The onset of dissection was ambiguous, though he had been suffering persistent back pain that started at age 13 years while practicing judo, but was never referred to a hospital. His family history was notable for aortic and vascular diseases (Fig. 1; Supp. Table S1), and he had two relatives, an uncle (Patient III:3) who died of acute dissection of the thoracoabdominal aorta at the age of 45 years and a cousin (Patient IV:1) who experienced aortic dissections at the age of 34 years. Furthermore, his aunt (Patient III:1), another cousin (Patient IV:7), and a first cousin once removed (Patient III:8) had severe or surgically repaired aortic aneurysms. Three other relatives (Patients III:2, II:1, and II:2), including his father, died suddenly of an unknown etiology in their 40 s.

His physical findings were unremarkable, as there were no ocular, skin, or cardiac abnormalities. Echocardiogram results revealed a moderately dilated aortic diameter at the sinuses of Valsalva (left ventricle outflow tract diameter [LVOT] 22 mm, aortic diameter at the sinuses of Valsalva [AoSV] 36 mm, and aortic diameter at the supraaortic ridge [AoSAR] 30 mm).

Two other affected relatives (Patients III:8 and IV:7) were also examined, both of whom had no ocular, skin, or cardiac

abnormalities. Echocardiogram results revealed that Patient III:8 had a dilated aortic diameter at the sinuses of Valsalva (LVOT 23 mm, AoSV 51 mm, AoSAR 44 mm, and aortic diameter at ascending aorta [AoAA] 43 mm). In addition, Patient IV:7 was shown to have a moderately dilated aortic diameter at the sinuses of Valsalva (LVOT 19 mm, AoSV 36 mm, AoSAR 29 mm, and AoAA 30 mm).

Histological examination of surgically removed aortic tissues from Patients IV:5 and IV:7 revealed a disorganized medial fiber structure or cystic medial necrosis (Supp. Fig. S1).

Sporadic Case (M80)

A heterozygous A to G transition at cDNA position 140 in exon 5 of the *ACTA2* gene was detected. This mutation predicts an amino acid substitution of Tyr 145 to Cys, and was not detected in the rest of the cohort or in 190 control subjects. Tyr145 has been shown to be one of the gelsolin binding sites, along with Gly148, Glu169, Gly344, Ile347, Leu348, Leu351, Ser352, and Thr353, and it faces the hydrophobic cleft between subdomains 1 and 4 [Dominguez, 2004] (Fig. 3C). They are all highly-conserved amino acids in the actin family and bind to gelsolin, a key regulator of actin filament assembly and disassembly, by capping and severing F-actin. The substitution of Tyr145 to Cys is expected to perturb the integrity of ligand binding, as shown with previously reported p.R149C and p.T353N (Fig. 3C).

The patient was a 31-year-old male who suffered an acute dissection in the descending aorta (Stanford B type) and was treated conservatively with antihypertensive therapy (Supp. Table S1). He had another acute dissection in the proximal descending aorta 1 year later, followed by graft replacement of the total descending aorta. He became obese (175 cm, 117 kg, body mass index 38.2) after stopping participation in amateur wrestling at the age of 23 years and had mild hypertension, hypercholesterolemia (285 mg/dl), and hyperuricemia (11.8 mg/dl). His family history was unremarkable, and there were no instances of aortic dissection or sudden death. Due to obesity, the echocardiogram examination was incomplete; however, the aortic diameters at the sinuses of Valsalva were not remarkable (AoSV 35 mm, and AoAA 30 mm). Histological examination of surgically removed aortic tissues revealed cystic medial necrosis (Supp. Fig. S1). Unfortunately, physical examination findings and genetic analyses of other family members were unavailable.

Discussion

In the present study, we confirmed that *ACTA2* mutations are an important cause of familial AADs. In a total of 14 probands analyzed, we identified three mutations in three unrelated families, for a ratio of 21%. In a study of a cohort of 97 TAAD families, Guo et al. [2007] argued that *ACTA2* mutations are the most common cause of familial TAAD yet found and are responsible for 14% of reported cases. Our data support their conclusion regarding that point, even though the study design was different. In addition, our analysis of 26 additional sporadic and young-onset TAAD cases identified one mutation that is thought to affect ligand binding characteristics.

Of the four mutations identified in the present study, three were novel. One of these mutations, p.R149C, is the same as reported by Guo et al. [2007] and the clinical presentation was similar, as the patient had livedo reticularis and an iris cyst. The second mutation, c. 616+1G>T, was novel and found to affect mRNA splicing by skipping entire exon 6, resulting in 54 amino acid deletions. It should be unequivocally causative, since a transcribed peptide will lack several important binding sites of known molecules, including ATP, gelsolin, and profilin. The third mutation, p.R212Q, was also novel, and our findings that it affected family members in more than three generations and was located to face the ATP binding cleft suggest it to be a causative mutation. The fourth mutation, p.Y145C, was identified in a nonfamilial case and was also novel. Unfortunately, additional investigations such as a genetic study of his parents could not be performed. Nevertheless, based on the finding showing substitution of gelsolin-binding Tyr, which was previously reported in several structural analyses, we concluded that this mutation was also causative. Although further investigation is needed, we consider that the corresponding *ACTA2* mutation causes deterioration of structural integrity at the cellular level.

We found a higher rate of aortic dissection in the descending portion in patients with the *ACTA2* mutation as compared with previous reports [Guo et al., 2007]. Of 11 dissection events in which the dissection type was proven, six were Stanford type B and five were type A. In the former six patients, at least three were known to be absent of annuloaortic ectasia (AAE) or involvement of the ascending portion of the aorta. This is a significant contrast, since most cases of Marfan syndrome have aortic involvement in the ascending portion, especially the sinus of Valsalva [Boileau et al., 1993; De Paepe et al., 1996; Faivre et al., 2007]. On the other hand, three affected individuals in Family 3 showed only AAE without any dilatation in the descending aorta. In the previous report by Guo et al. [2007], there were 19 aneurysms in the ascending portion, 36 type A dissections, and 13 type B dissections, indicating more type A events than in our study. One possible explanation for this discrepancy is the different mutation types found.

In addition, we found that the extravascular involvements described in the previous report, livedo reticularis and iris folliculi, were rare in our study. Although these features were noted in a patient with the p.R149C mutation, which is the same as in a previous report, no other affected individuals were noted with these features. This may be another mutation-specific feature, since ocular involvements were noted solely with the p.R149C mutation in that previous report.

Interestingly, four patients in our study were former athletes, two tennis players, a judo wrestler, and an amateur wrestler, who actively played sports in their teens before the aortic events occurred. Although there is no evidence, physical contact or higher circulation performance during sports participation might be an additional causative mechanism for aortic events.

While we were revising this report, Guo et al. [2009] reported additional *ACTA2* mutations including p.R212Q in familial TAAD. In addition, they indicated that *ACTA2* mutation carriers can have a diversity of vascular diseases, including premature onset of coronary artery disease and premature ischemic stroke, as well as TAAD. However, we did not find any specific clinical feature suggesting premature onset of coronary artery disease or premature ischemic strokes, though some of family members (Family 2, Patients II:1 and II:2; and Family 3, Patients II:1 and II:2) died suddenly, some with chest pain. Furthermore, we did not find any individual with the *ACTA2* mutation and without aortic disease. Those clinical features require further evaluations using individuals in those families over a long period of time.

In conclusion, our data confirmed that *ACTA2* mutations are important in familial TAAD. Furthermore, we report the first nonfamilial TAAD case with an *ACTA2* mutation. Since the first

and only clinical symptom for these patients was an AAD, which can be life-threatening, identification of mutations in family members of patients with an *ACTA2* mutation would be beneficial in regard to clinical aspects for improved surveillance and awareness of treatment, as well as consideration of social, psychological, and ethical issues. We think that genetic analysis of *ACTA2* for patients with familial TAAD or young-onset TAAD is as clinically as important as that of *FBN1* and *TGFBR*s.

Acknowledgments

We thank Ms. Aya Narita, Ms. Yoko Miyamoto, and other members of the Department of Bioscience for their technical support with this study. We also thank the patients for their participation and members of the Divisions of Cardiovascular Medicine and Surgery for their patient care. This work was supported in part by a Grant for the Promotion of Fundamental Studies in Health Science from the Organization for Pharmaceutical Safety and Research (OPSR) of Japan and a grant from the Program for Promotion of Fundamental Studies in Health Sciences of the National Institute of Biomedical Innovation (NIBIO), as well as Grants-in-Aid for Scientific Research from Japan Society for the Promotion of Science, and Research Grants for Cardiovascular Diseases from the Ministry of Health, Labour and Welfare, Japan.

References

Albornoz G, Coady MA, Roberts M, Davies RR, Tranquilli M, Rizzo JA, Elefteriades JA. 2006. Familial thoracic aortic aneurysms and dissections—incidence, modes of inheritance, and phenotypic patterns. Ann Thorac Surg 82:1400–1405.

Biddinger A, Rocklin M, Coselli J, Milewicz DM. 1997. Familial thoracic aortic dilatations and dissections: a case control study. J Vasc Surg 25:506–511.

Boileau C, Jondeau G, Babron MC, Coulon M, Alexandre JA, Sakai L, Melki J, Delorme G, Dubourg O, Bonaiti-Pellie C, Bourdarias JP, Junien C. 1993. Autosomal dominant Marfan-like connective-tissue disorder with aortic dilation and skeletal anomalies not linked to the fibrillin genes. Am J Hum Genet 53:46–54.

Coady MA, Davies RR, Roberts M, Goldstein LJ, Rogalski MJ, Rizzo JA, Hammond GL, Kopf GS, Elefteriades JA. 1999. Familial patterns of thoracic aortic aneurysms. Arch Surg 134:361–367.

De Paepe A, Devereux RB, Dietz HC, Hennekam RC, Pyeritz RE. 1996. Revised diagnostic criteria for the Marfan syndrome. Am J Med Genet 62:417–426.

Dietz HC, Cutting GR, Pyeritz RE, Maslen CL, Sakai LY, Corson GM, Puffenberger EG, Hamosh A, Nanthakumar EJ, Curristin M, Stetten G, Meyers DA, Francomano CA. 1991. Marfan syndrome caused by a recurrent de novo missense mutation in the fibrillin gene. Nature 352:337–339.

Dominguez R. 2004. Actin-binding proteins—a unifying hypothesis. Trends Biochem Sci 29:572–578.

Faivre L, Collod-Beroud G, Loeys BL, Child A, Binquet C, Gautier E, Callewaert B, Arbustini E, Mayer K, Arslan-Kirchner M, Kiotsekoglou A, Comeglio P, Marziliano N, Dietz HC, Halliday D, Beroud C, Bonithon-Kopp C, Claustres M, Muti C, Plauchu H, Robinson PN, Adès LC, Biggin A, Benetts B, Brett M, Holman KJ, De Backer J, Coucke P, Francke U, De Paepe A, Jondeau G, Boileau C. 2007. Effect of mutation type and location on clinical outcome in 1,013 probands with Marfan syndrome or related phenotypes and *FBN1* mutations: an international study. Am J Hum Genet 81:454–466.

Garg V, Muth AN, Ransom JF, Schluterman MK, Barnes R, King IN, Grossfeld PD, Srivastava D. 2005. Mutations in *NOTCH1* cause aortic valve disease. Nature 437:270–274.

Guex N, Peitsch MC. 1988. SWISS-MODEL and the Swiss-PdbViewer: an environment for comparative protein modeling. Electrophoresis 18:2714–2723.

Guo DC, Pannu H, Tran-Fadulu V, Papke CL, Yu RK, Avidan N, Bourgeois S, Estrera AL, Safi HJ, Sparks E, Amor D, Ades L, McConnell V, Willoughby CE, Abuelo D, Willing M, Lewis RA, Kim DH, Scherer S, Tung PP, Ahn C, Buja LM, Raman CS, Shete SS, Milewicz DM. 2007. Mutations in smooth muscle alpha-actin (ACTA2) lead to thoracic aortic aneurysms and dissections. Nat Genet 39:1488–1493.

Guo DC, Papke CL, Tran-Fadulu V, Regalado ES, Avidan N, Johnson RJ, Kim DH, Pannu H, Willing MC, Sparks E, Pyeritz RE, Singh MN, Dalman RL, Grotta JC, Marian AJ, Boerwinkle EA, Frazier LQ, LeMaire SA, Coselli JS, Estrera AL, Safi HJ, Veeraraghavan S, Muzny DM, Wheeler DA, Willerson JT, Yu RK, Shete SS, Scherer SE, Raman CS, Buja LM, Milewicz DM. 2009. Mutations in smooth muscle alpha-actin (ACTA2) case coronary artery disease, stroke, and Moyamoya disease, along with thoracic aortic disease. Am J Hum Genet 84:617–627.

Loeys BL, Chen J, Neptune ER, Judge DP, Podowski M, Holm T, Meyers J, Leitch CC, Katsanis N, Sharifi N, Xu FL, Myers LA, Spevak PJ, Cameron DE, De Backer J, Hellemans J, Chen Y, Davis EC, Webb CL, Kress W, Coucke P, Rifkin DB, De Paepe AM, Dietz HC. 2005. A syndrome of altered cardiovascular, craniofacial, neurocognitive and skeletal development caused by mutations in *TGFBR1* or *TGFBR2*. Nat Genet 37:275–281.

Mizuguchi T, Collod-Beroud G, Akiyama T, Abifadel M, Harada N, Morisaki T, Allard D, Varret M, Claustres M, Morisaki H, Ihara M, Kinoshita A, Yoshiura K, Junien C, Kajii T, Jondeau G, Ohta T, Kishino T, Furukawa Y, Nakamura Y, Niikawa N, Boileau C, Matsumoto N. 2004. Heterozygous *TGFBR2* mutations in Marfan syndrome. Nat Genet 36:855–860.

Page R, Lindberg U, Schutt CE. 1998. Domain motions in actin. J Mol Biol 280:463–474.

Pannu H, Avidan N, Tran-Fadulu V, Milewicz DM. 2006. Genetic basis of thoracic aortic aneurysms and dissections: potential relevance to abdominal aortic aneurysms. Ann NY Acad Sci 1085:242–255.

Pannu H, Tran-Fadulu V, Papke CL, Scherer S, Liu Y, Presley C, Guo D, Estrera AL, Safi HJ, Brasier AR, Vick GW, Marian AJ, Raman CS, Buja LM, Milewicz DM. 2007. MYH11 mutations result in a distinct vascular pathology driven by insulin-like growth factor 1 and angiotensin II. Hum Mol Genet 16:2453–2462.

Ramensky V, Bork P, Sunyaev S. 2002. Human non-synonymous SNPs: server and survey. Nucleic Acids Res 30:3894–3900.

Superti-Furga A, Gugler E, Gitzelmann R, Steinmann B. 1988. Ehlers-Danlos syndrome type IV: a multi-exon deletion in one of the two COL3A1 alleles affecting structure, stability, and processing of type III procollagen. J Biol Chem 263:6226–6232.

Vorobiev S, Strokopytov B, Drubin DG, Frieden C, Ono S, Condeelis J, Rubenstein PA, Almo SC. 2003. The structure of nonvertebrate actin: implications for the ATP hydrolytic mechanism. Proc Natl Acad Sci USA 100:5760–5765.

Zhu L, Vranckx R, Van Kien PK, Lalande A, Boisset N, Mathieu F, Wegman M, Glancy L, Gasc JM, Brunotte F, Bruneval P, Wolf JE, Michel JB, Jeunemaitre X. 2006. Mutations in myosin heavy chain 11 cause a syndrome associating thoracic aortic aneurysm/aortic dissection and patent ductus arteriosus. Nat Genet 38:343–349.

Acta Biomaterialia 6 (2010) 403–408

Contents lists available at ScienceDirect

Acta Biomaterialia

journal homepage: www.elsevier.com/locate/actabiomat

Preparation of a collagen/polymer hybrid gel designed for tissue membranes. Part I: Controlling the polymer–collagen cross-linking process using an ethanol/water co-solvent

Kwangwoo Nam [a,b], Tsuyoshi Kimura [a,b], Seiichi Funamoto [a], Akio Kishida [a,b,*]

[a] Division of Biofunctional Molecules, Institute of Biomaterials and Bioengineering, Tokyo Medical and Dental University, 2-3-10 Kanda-Surugadai, Chiyoda-ku, Tokyo 101-0062, Japan
[b] JST-CREST, Honcho, Kawaguchi, Saitama 332-0012, Japan

ARTICLE INFO

Article history:
Received 5 January 2009
Received in revised form 11 May 2009
Accepted 11 June 2009
Available online 14 June 2009

Keywords:
Collagen
Cross-link
Phospholipid polymer
Hydrogel

ABSTRACT

The drawback with collagen/2-methacryloyloxyethyl phosphorylcholine (MPC) polymer hybrid gels (collagen/phospholipid polymer hybrid gels) prepared in alkaline morpholinoethane sulfonic acid (MES) aqueous solution is that the cross-linking rate between the polymer and the collagen is low. To solve this problem, ethanol has been adopted as the reaction solvent, to prevent 1-ethyl-3-(3-dimethylaminopropyl)-1-carbodiimide hydrochloride (EDC) hydrolysis. Alterations in the ethanol mole concentration changed the cross-linking rate between the MPC polymer and the collagen gel. Prevention of EDC hydrolysis is clearly observed; protonation of carboxyl groups implies that the ratio of ethanol to water should be controlled. The polymer shows signs of penetration into the collagen gel layer, thus forming a totally homogeneous phase gel. This affects the mechanical strength of the collagen gel, making the gel much stiffer and brittle with an increase in the swelling ratio, as compared with that prepared in MES buffer. However, it is possible to obtain a collagen/phospholipid polymer hybrid gel with a high polymer portion and the cross-linking rate can be successfully controlled.

1. Introduction

Collagen is the major constituent of connective tissues and is widely used in biomaterial applications [1–4]. The use of collagen as a biomaterial offers advantages such as biocompatibility, low toxicity and natural abundance, in addition to well-documented structural, physical, chemical and immunological properties [5]. However, purified collagen possesses weak mechanical properties, which are inadequate for application as a biomaterial. The formation of covalent intermolecular cross-links between collagen molecules in macromolecular fibrils with appropriate biocompatible molecules is an effective method of improving mechanical integrity and stability [6–9].

Covalent cross-linking using 1-ethyl-3-(3-dimethylaminopropyl)-1-carbodiimide hydrochloride (EDC) and N-hydroxysuccinimide (NHS) is a widely used method. The coupling reaction produces "zero length" amide cross-links between carboxylic acid groups and amine groups; this reduces side-effects that may be induced by a cross-linking agent [10]. In addition, adoption of an additional polymer that contains a carboxyl group enables the cross-linking of collagen and the polymer using EDC and NHS to reinforce the mechanical strength of the collagen gel.

By coupling to anti-coagulant substances, such as heparin, it is possible to provide collagen with properties such as hemocompatibility, which collagen alone does not possess [11]. However, the conditions under which the coupling reaction cross-links the collagen and the polymer to control a particular property remain unclear. We adopted 2-methacryloyloxyethyl phosphorylcholine (MPC) polymer, which has good hemocompatibility. We succeeded in preparing an MPC polymer immobilized collagen gel using [poly(MPC-co-methacrylic acid)] (PMA) and EDC/NHS in 0.05 M 2-morpholinoethane sulfonic acid (MES) buffer (pH 9.0), as explained in our previous report [12]. We expected the immobilized MPC polymer to express good hemocompatibility and non-cell adhesive properties, but the immobilized fraction of MPC head groups was low, implying that cross-linking did not occur efficiently and gel could not be applied as a tissue membrane.

To solve the above mentioned problem we adopted ethanol as the reaction solvent, because hydrolysis of EDC in water occurs over a very short timespan [13,14] and it has been predicted that ethanol may prevent this hydrolysis. The use of ethanol has been reported by many researchers, but its reactivity has not yet been focused upon [15–17]. In a previous study, we adopted an ethanol/water co-solvent to prepare a collagen gel using EDC and NHS. We found that the ethanol/water co-solvent did not affect the collagen triple helix

* Corresponding author. Address: Division of Biofunctional Molecules, Institute of Biomaterials and Bioengineering, Tokyo Medical and Dental University, 2-3-10 Kanda-Surugadai, Chiyoda-ku, Tokyo 101-0062, Japan. Tel./fax: +81 03 5841 8028.
E-mail address: kishida.fm@tmd.ac.jp (A. Kishida).

1742-7061/$ - see front matter © 2009 Acta Materialia Inc. Published by Elsevier Ltd. All rights reserved.
doi:10.1016/j.actbio.2009.06.021

until the ethanol mole concentration (N_A) reached ~0.42 (70 vol.% ethanol) [18]. The reactivity of EDC with the carboxylate anion groups of collagen helices could be enhanced by the ethanol/water co-solvent, but the concentration ranged from $N_A \sim 0.07–0.17$ (~10–40 vol.% ethanol) because a balance between hydrolysis of EDC and protonation of carboxylate anions had to be maintained.

To apply this method to polymer–collagen cross-linking we first characterized the physical behavior of the MPC polymers and poly(methacrylate) in the ethanol/water co-solvent in order to investigate the reactivities of EDC and NHS with the polymers. For MPC polymers we selected two types of PMA: PMA30 [30 mol.% MPC, 70 mol.% methacrylic acid (MA)] and PMA90 (90 mol.% MPC, 10 mol.% MA). Subsequently we cross-linked the polymer with collagen to characterize network formation by the collagen gel in the ethanol/water co-solvent. In this manner we attempted to establish a theory of the polymer–collagen gel cross-linking system for preparation of a tissue membrane based on collagen. The second phase of the study, which involved characterization of the biological properties, will be reported in part II.

2. Materials and methods

2.1. Preparation of the collagen/phospholipid polymer hybrid gels (MiC gels)

PMA was synthesized according to a previously published method [12,19]. In brief, MPC and MA were co-polymerized in ethanol solution for 16 h at 60 °C using 2,2-azobisisobutyronitrile as initiator. The molar ratios of PMA were MPC:MA 3:7 (PMA30) and 9:1 (PMA90) and the average molecular weights were 3.2×10^5 and 4.5×10^5.

Cross-linked collagen gel was prepared using a previously reported method [12,18,19]. Instead of 0.5 wt.% collagen type I solution (pH 3) (KOKEN, Tokyo, Japan), 2 wt.% collagen type I aqueous solution was prepared and used for film preparation (thickness 50 ± 3 μm). The collagen/phospholipid polymer hybrid gel (MiC gel) was prepared using collagen film. PMA30 and PMA90 were added to the ethanol/water co-solvent series (ethanol mole concentration N_A = ~0–0.32), along with EDC and NHS. The polymer was activated for 10 min before the collagen film was immersed in the solvent. The molar ratios of each chemical were fixed – EDC:NHS:collagen carboxylic acid groups 10:10:1. Immobilization of PMA to collagen was allowed to continue for 24 h at 4 °C to form a MiC30 (cross-linked with PMA30) gel and MiC90 (cross-linked with PMA90) gel. To evaluate the physical properties, a collagen film stabilized in MES buffer, pH 9.0, was prepared (Uc gel). The basic preparation scheme and an image of the MiC30 gel are shown in Fig. 1. The abbreviations for the collagen gels used in this study are listed in Table 1.

2.2. Characterization of the polymers

The molecular sizes of PMA00, PMA30 and PM90 were measured using a dynamic scattering method using a Zetasizer light scattering system (Malvern Instruments Ltd., Malvern, UK) equipped with a He–Ne laser (λ = 633 nm, 4.0 mW) at 25 °C. The samples were prepared in an ethanol/water co-solvent series with a concentration of 1 mg ml^{-1}. The viscosity and transparency of the ethanol/water co-solvent series were calculated for precise measurement of molecule size. The ζ potential of the polymers measured using the same instrument was executed after mathematical calculation of the permittivity of the co-solvents [20]. All samples were filtered through a 0.45 μm Millex filter (Millipore, Bedford, MA) before measurement.

2.3. Characterization of the MiC gels

2.3.1. Surface analysis

Surface analysis was performed using X-ray photoelectron spectroscopy (XPS) (AXIS-HSi, Shimadzu/KRATOS, Kyoto, Japan). Samples that had been cut into small pieces (2 × 2 cm) were lyophilized overnight (FDU-2000, EYELA, Tokyo, Japan). The chemical composition of the gel surface was determined from the release angle of photoelectrons fixed at 30°.

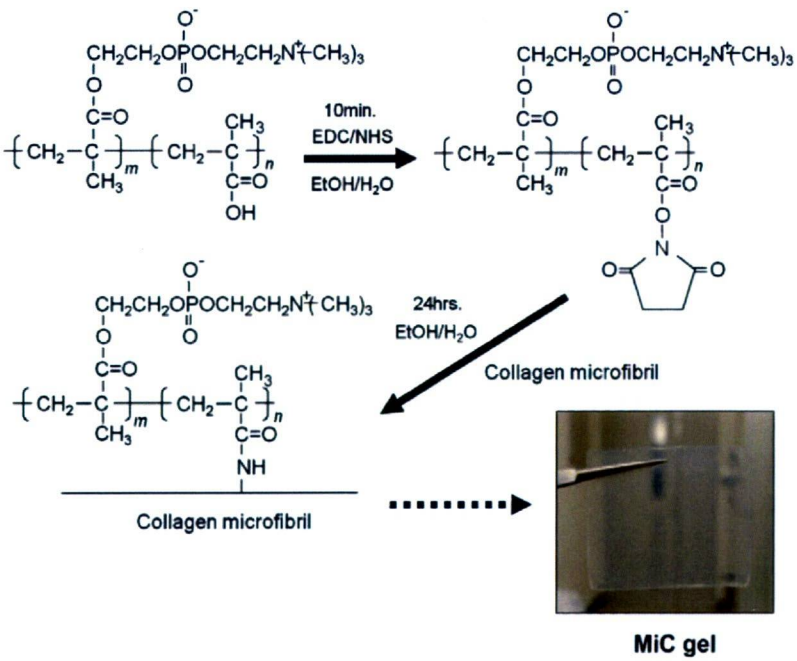

Fig. 1. Basic preparation scheme and image of the MiC gel.

Table 1
Abbreviations of polymers and collagen gels used in this study.

Sample abbreviation	
PMA00	MPC:MA = 0:10
PMA30	MPC:MA = 30:70
PMA90	MPC:MA = 90:10
MiC30 gel	Collagen gel cross-linked with PMA30 in water/ethanol co-solvent
MiC90 gel	Collagen gel cross-linked with PMA90 in water/ethanol co-solvent
CoPho gel	Collagen gel cross-linked with PMA30 in MES buffer
Uc gel	Collagen gel stabilized in alkaline pH aqueous solution (pH ≈ 9.0)

2.3.2. Determination of the reacted amine group content

The concentration of primary amine groups in tissue samples was determined using a colorimetric assay [21,22]. Three to four milligrams of each sample were prepared. The samples were then placed in aqueous $NaHCO_3$ solution (Kanto Chemicals, Tokyo, Japan) and 2,4,6-tri-nitrobenzene sulfonic acid (TNBS) (Wako Chemicals, Osaka, Japan). The reaction was allowed to proceed for 2 h at 40 °C, The samples were then rinsed with saline solution to remove unreacted TNBS. Subsequent to freeze-drying the samples overnight, the dry mass was determined. The dry samples were immersed in 6 M aqueous HCl until they were fully dissolved. The resultant solution was subsequently diluted with distilled water and the absorbance was measured at 345 nm using an ultraviolet spectrophotometer (V-560, Jasco, Tokyo, Japan) to calculate the concentration of reacted amine groups [18,21–23]. All the data were calculated from the percentage reacted amine group content of the respective collagen gels by assuming that the amine groups of Uc gel reacted 100% [23]. The values obtained were used to estimate the free amine group content.

2.3.3. Mechanical test

The stress–strain curves for the Uc and MiC30 gels (N_A = ~0–0.32) was determined by means of uniaxial measurements performed using a universal testing machine (Rheoner II, Yamaden, Tokyo, Japan). The size of the samples was 3 × 1 cm. Each sample was strained at a rate of 0.5 cm s^{-1} with a force of 20 N. The test was repeated three times and average values were obtained. The data were processed and the strain–stress curves were compared with that of the Uc gel.

2.3.4. Swelling test

Swelling test on the samples was executed by cutting the lyophilized gels into small pieces and placing them in distilled water at 25 °C. The gels were gently shaken for 24 h and were measured to assess the change in weight of the sample. The swelling ratio was calculated in order to define the phenomenon of swelling accomplished by water absorption. The experiment was repeated five times and average values were calculated, along with estimations of standard deviations. The following equation was used to calculate the swelling ratio [24]:

$$\text{swelling ratio } S(\%) = \frac{W_h - W_d}{W_d} \times 100, \quad (1)$$

where W_h denotes the hydrated weight of the gel and W_d denotes the dry weight of the gel.

2.4. Statistical analysis

All experiments were repeated at least three times (five times for ζ potential analysis and size calculation) and the values are expressed as means ± standard deviations. Statistical analysis was performed using ANOVA, with the significant level set at $P < 0.05$.

3. Results

Fig. 2a shows the change in size of the polymer with respect to the ethanol mole concentration. The size increases with increasing ethanol mole concentration. The increase was more significant when poly(methacrylate) homopolymer (PMA00) was used. This is clearly shown in Fig. 2b, in which the sizes of the respective polymers are normalized. PMA90, which contains 90% MPC head group, had the largest molecular size in water, but its size did not increase as much as those of PMA00 and PMA30 with increasing ethanol mole concentration. The sizes of PMA30 and PMA90 after $N_A \sim 0.32$ were not measured because they precipitated at higher ethanol mole concentrations.

Fig. 3 shows the change in ζ potential with respect to ethanol mole concentration. It can be seen that the carboxyl groups of PMAs exist as carboxylate anions under aqueous conditions and that the addition of ethanol to water protonates these carboxylate anions. The change in ζ potential is larger for PMA00 and PMA30 as compared with that for PMA90.

Fig. 4 shows the free amine group content (Fig. 4a) and phosphorus atomic concentration (Fig. 4b) of the MiC30 and MiC90 gels. The lowest free amine group content and highest phosphorus atomic concentration were obtained for $N_A \sim 0.12$ (30 vol.% ethanol). The free amine group content was lower for MiC90 than for MiC30, but the phosphorus atomic concentration was lower than that of MiC30. Cross-linking between PMA00 and collagen did not occur because of precipitation of the polymer.

Fig. 5 shows the mechanical strength of the MiC30 gel prepared at various ethanol mole concentrations between 0 and 0.42*n*. The gel shows an approximately 6-fold increase in the Young's modulus as compared with the Uc gel. However, the Young's moduli of

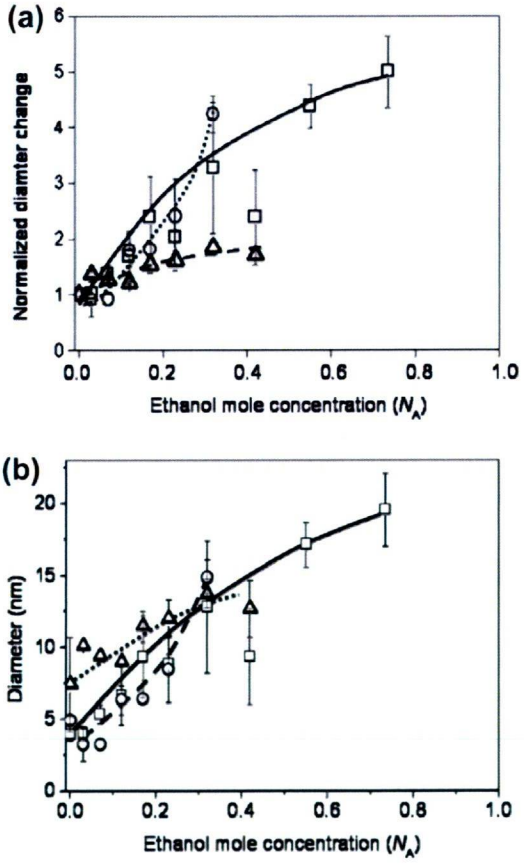

Fig. 2. (a) The diameters of PMA00, PMA30 and PMA90 and (b) changes in the normalized diameters of PMA00, PMA30 and PMA90 with changing ethanol mole concentration. -□-, PMA00; -○-, PMA30; -△-, PMA90. Each value represents the mean ± SD (n = 5).

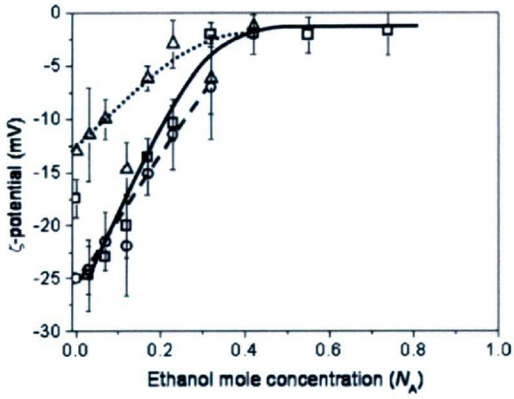

Fig. 3. Relationship between the ζ potential of PMA00, PMA30 and PMA90 and ethanol mole concentration. -□-, PMA00; -○-, PMA30; -△-, PMA90. Each value represents the mean ± SD (n = 5).

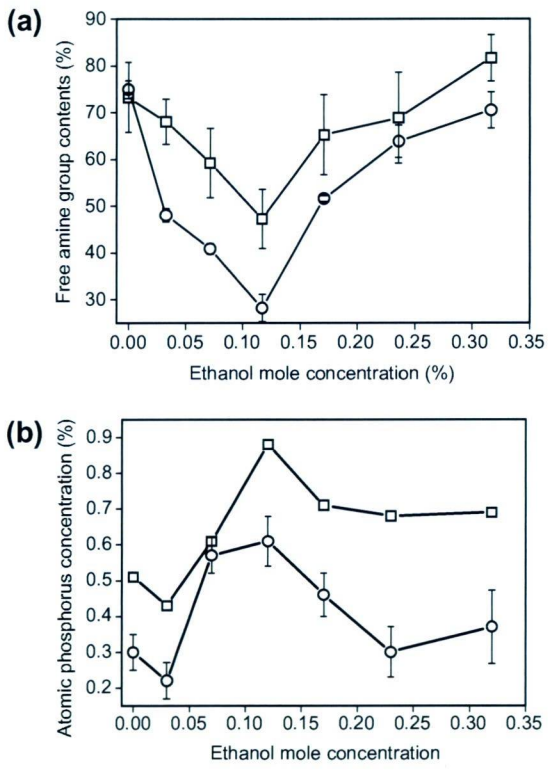

Fig. 4. Relationship between the free amine group content (a) and atomic phosphorus concentration (b) of the MiC30 and MiC90 gels and ethanol mole concentration. □, MiC30; ○, MiC90. Each value represents the mean ± SD (n = 5).

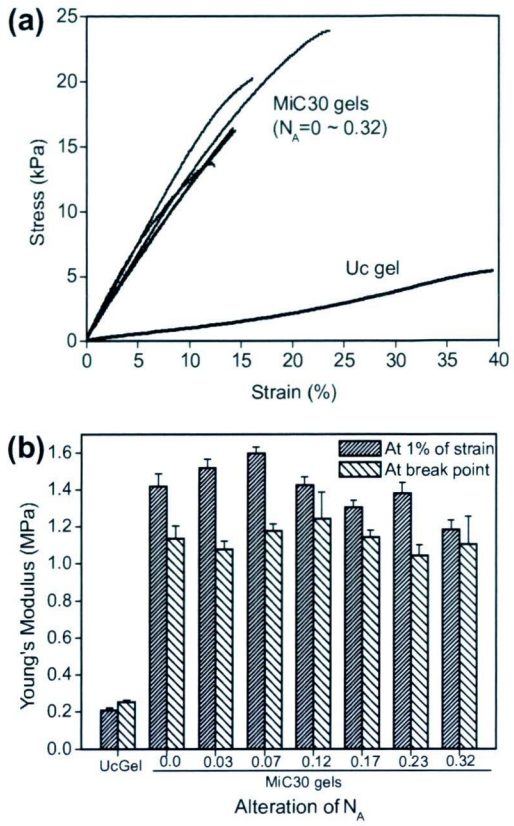

Fig. 5. (a) Stress–strain curve for the MiC30 gels with respect to ethanol mole concentration during preparation and (b) the relationship between Young's modulus and the ethanol/water co-solvent at 1% strain and at break (N_A = 0–0.32).

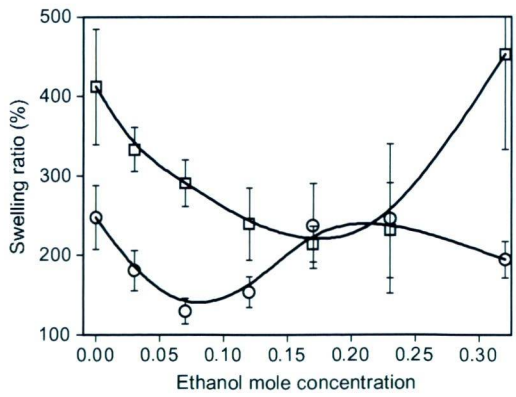

Fig. 6. Relationship between the swelling ratios of the MiC30 and MiC90 gels and ethanol mole concentration. □, MiC30; ○, MiC90. Each value represents the mean ± SD (n = 5).

the MiC30 gels prepared at different ethanol mole concentrations did not show significant differences. The Young's moduli at 1% strain and at break are shown at Fig. 5b. The viscoelasticity is not shown for MiC30 gels, whereas the Uc gel showed clear but low viscoelasticity. The mechanical strength of the MiC90 gels did not show much difference compared with the MiC30 gels (data not shown).

Fig. 6 shows the swelling ratios of the MiC30 and MiC90 gels, for which the swelling ratios were approximately three times those of gels prepared in MES buffer, but lower than the Uc gel [12,19]. The swelling ratio of MiC90 gel was lower than that of MiC30 gel. The concentration producing the lowest swelling ratio did not match the free amine group content or the phosphorus atomic concentration.

4. Discussion

4.1. Characterization of PMA

Collagen intrahelical cross-linking can be altered by ethanol mole concentration because hydrolysis of EDC can be prevented,

but protonation of carboxylate anions is promoted [18]. In order to investigate whether or not it is possible to directly apply our theory of collagen cross-linking to the polymer–collagen, the states of the polymer and EDC in the ethanol/water co-solvent were characterized using dynamic light scattering.

MPC polymer is hydrophilic, which results in expansion of the polymer in water. PMA90, which consists of 90% MPC moiety within the polymer chain, has the greatest hydrodynamic volume, whereas PMA00, which consists of pure methacrylic acid, has the lowest hydrodynamic volume. As the ethanol mole percentage increases, the MPC head group starts to aggregate. This is attributed to an increase in the hydrophobicity of the solvent. However, the aggregation does not decrease the hydrodynamic volume effectively until the ethanol mole percentage reaches 0.32. Kiritoshi and Ishihara have reported that, using a MPC hydrogel, the volume of the MPC hydrogel decreased rapidly when the ethanol volume percentage was higher than 70% ($N_A \sim 0.42$), thereby leading to collapse of the hydrogel [25,26]. In the dissolution experiment we found that PMA90 and PMA30 precipitated at this concentration. This implies that there exists a threshold concentration for sudden collapse of MPC polymers, which is formed by the aggregation of MPC head groups. PMA00 does not show precipitation or a decrease in the hydrodynamic volume. Instead, expansion of the polymer chain continues until $N_A \sim 0.73$.

It should be noted that all polymers increase in hydrodynamic volume with increasing ethanol mole concentration. This is due to the formation of neutral carboxyl groups in the presence of ethanol, as shown in Fig. 3. However, hydrogen bonds between the carboxyl groups cannot be formed due to cleavage of hydrogen bonds under hydrophobic conditions [27]. Expansion of the hydrodynamic volume is considered to be caused by cleavage of hydrogen bonds, providing a greater free space between the molecules [28,29]. The formation of neutral carboxyl groups indicates that expansion of the polymer occurs due to carboxyl acid groups in the sidechain. Fig. 2b supports this argument, as the lowest increase in hydrodynamic volume was observed for PMA90 (with a 2-fold increment) and the highest increase was observed for PMA00 (with a 4-fold increment). The hydrodynamic volume in pure water indicates that PMA90 is largest due to the bulky MPC head groups. Hence, it is considered that the increase in ethanol concentration increases the hydrodynamic volume and the formation of carboxyl groups.

4.2. Characterization of MiC gels

In the case of PMA–collagen cross-linking the highest cross-linking rate was observed at $N_A \sim 0.12$, at which the same ethanol mole concentration was required for triple helix intrahelical cross-linking (Fig. 4) [18]. Although the cross-linking rate was greater for the MiC90 gel, the phosphorus atomic concentration was lower. This implies that the activation of carboxyl groups on the polymer and collagen due to EDC occur contemporaneously. Since the number of carboxyl groups was lower for PMA90, EDC that does not participate in polymer activation participates in collagen activation, i.e. the polymer–collagen network and intrahelical cross-links exist together. The lowest level of possible unreacted amine groups was produced when EDC/NHS and polymer were used for cross-linking, with approximately 28% of free amine groups. Cross-linking of PMA00 and collagen is impossible because addition of EDC to the PMA00 solution caused immediate precipitation.

When the polymer was immobilized on the surface of the collagen gel (CoPho gel), the strain–stress curve increased compared with that of the physically cross-linked gel, but it maintained its viscoelasticity with a low elastic modulus [19]. However, the case of the physically cross-linked gel was shown to be different. The increase in Young's modulus was confirmed, but the stress–strain curve showed clear brittle plastic behavior (Fig. 5a). The Young's modulus at the breakpoint was lower than that at 1% strain. This implies that there is a difference between the CoPho gel and the physically cross-linked gel, i.e. molecular penetration of PMA into the CoPho gel occurred. The polymer penetrated the collagen layer and the mechanical properties of MPC polymer appear very clearly. Differences with regard to ethanol mole concentration could not be detected (Fig. 5b). This is because the factor that directly affects the mechanical strength is the polymer blended with collagen, rather than the number of cross-links. The above argument can be confirmed by measuring the swelling ratio. As shown in Fig. 6, the swelling ratios of the collagen gels increased beyond 150% in the water/ethanol co-solvent. In the case of collagen gels prepared in MES buffer the swelling ratio was below 120% [12]. This implies that the collagen gel adsorbs water and the polymer contemporaneously during the coupling reaction. The polymers are positioned between the collagen molecules (triple helix structure, tertiary structure), connecting them. This is thought to be the reason for the low free amine group content as compared with gels prepared in MES buffer, because 35% free amine group content is considered too low to be achieved in collagen gel. A polymer chain located only on the surface of the collagen gel cannot decrease the free amine group content due to the existence of entangled collagen molecules [12,30,31]. The entangled collagen molecules exhibit viscoelastic behavior when strain is applied. However, the polymers placed between the collagen molecules form a collagen–polymer network, which decreases the free amine group content and exhibits brittle plastic behavior once strain is applied.

Why would a collagen gel swell higher when a polymer–collagen network is formed inside the gel? First, the formation of collagen gels in MES buffer prevented adsorption of the polymer by entanglement of the collagen molecules, inducing stability of the collagen gel. However, the effect of ethanol on the collagen molecules is weak and its structural properties are maintained [18,32–34], allowing the polymer to penetrate the collagen layer to form a homogeneous gel. The suppression of hydrolysis of EDC would make it possible for the polymer to cross-link with collagen molecules inside the collagen gel [18]. Second, the MPC head groups function as bulky sidechains, producing large vacant spaces between the collagen molecules when water is adsorbed into the collagen gel (schematic image shown in Scheme 1). Furthermore, the self-swelling property of the MPC polymer in ethanol/water mixtures (Fig. 2) causes the gel to swell much more as water penetrates the MiC30 and MiC90 gels. This implies a mismatch between the swelling ratio and the free amine group content (Figs. 2 and 6). Swelling relies on the volumetric properties of the MPC polymer and the collagen gel, which does not rely on cross-linking rate, similarly to the MiC30 gel prepared in MES buffer [19]. Furthermore, because solvent penetration does not vary significantly with respect to ethanol mole concentration until $N_A \sim 0.42$ [18], we consider that solvent diffusivity does not differ for the MiC30 and MiC90 gels.

5. Conclusion

Through this research it was possible to establish the coupling reaction mechanism between collagen and an MPC polymer containing carboxyl groups using EDC and NHS. The ethanol mole concentration in the polymer–collagen cross-linking reaction had to be controlled due to changes in the hydrolysis of EDC and the protonation of carboxylate anions. Cross-linking between the MPC polymer and collagen molecules occurred within the collagen gel, rather than at the surface of the collagen. This led directly to good biological performance, implying that this material is a suitable tissue membrane. In part II, we will report on the in vitro and in vivo

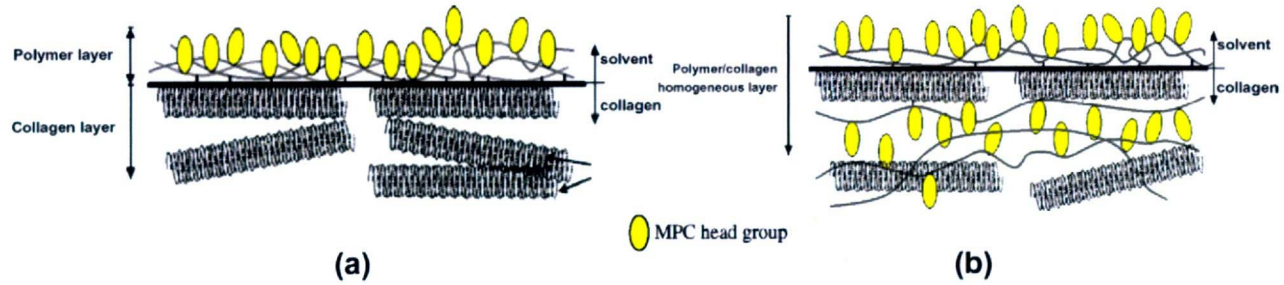

Scheme 1. Schematic image showing cross-linking of the polymer–collagen in MES buffer (a) and in ethanol/water co-solvent (b). Note the greater space created within the collagen gel by the MPC head groups.

behaviors of the MiC30 gels, which showed the highest PMA cross-linking rate.

Acknowledgements

This work supported in part by Grants-in-Aid from Research on Health Sciences focusing on Drug Innovation from the Japan Health Sciences Foundation, and Research on Human Genome, Tissue Engineering, Health and Labour Science Research Grant, Ministry of Health, Labour and Welfare, Japan. This work was also partly supported by a Grant-in-Aid from Core Research for Evolutional Science and Technology (CREST) of the Japan Science and Technology Agency (JST). We would like to thank Professor Kazuhiko Ishihara of The University of Tokyo for his kind assistance and advice on the preparation and analysis of the MPC polymer and Dr. James Sibarani of The University of Tokyo (presently at Udayana University, Indonesia) for his assistance with the XPS analysis.

Appendix. Figures with essential colour discrimination

Certain figures in this article, particularly Fig. 1 and Scheme 1, are difficult to interpret in black and white. The full colour images can be found in the on-line version, at doi: 10.1016/j.actbio.2009.06.021.

References

[1] Rao KP. Recent developments of collagen-based materials for medical applications and drug delivery systems. J Biomater Sci 1995;7:623–45.
[2] Friess W. Collagen-biomaterial for drug delivery. Eur J Pharm Biopharm 1998;45:112–36.
[3] Fujioka K, Maeda M, Hojo T, Sano A. Protein release from collagen matrices. Adv Drug Deliv Rev 1998;31:247–66.
[4] Lee CH, Singla A, Lee Y. Biomedical applications of collagen. Int J Pharm 2001;221:1–22.
[5] Duan X, Sheardown H. Crosslinking of collagen with dendrimers. J Biomed Mater Res 2005;75A:510–8.
[6] Nimni ME, Cheung D, Strates B, Kodama M, Sheikh K. Chemically modified collagen – a natural biomaterial for tissue replacement. J Biomed Mater Res 1987;21:741–71.
[7] Rault I, Frei V, Herbage D, Adbul-Marak NAH. Evaluation of different chemical methods for cross-linking collagen gel, films and sponges. J Mater Sci Mater Med 1996;7:215–21.
[8] Zeeman R, Dijkstra PJ, van Wachem PB, van Luyn MJ, Hendriks M, Cahalan PT, et al. Successive epoxy and carbodiimide cross-linking of dermal sheep collagen. Biomaterials 1999;20:921–31.
[9] Gentleman E, Lay AN, Dickerson DA, Nauman EA, Livesay GA, Dee KA. Mechanical characterization of collagen fibers and scaffolds for tissue engineering. Biomaterials 2003;24:3805–13.
[10] Wissink MJB. Endothelization of collagen matrices. Ph.D. thesis, University of Twente; 1999 [chapter 3].
[11] Wissink MJB, Beernink R, Pieper JS, Poot AA, Engbers GHM, Beugeling T, et al. Immobilization of heparin to EDC/NHS-crosslinked collagen. Characterization and in vitro evaluation. Biomaterials 2001;22:151–63.
[12] Nam K, Kimura T, Kishida A. Physical and biological properties of collagen–phospholipid polymer hybrid gels. Biomaterials 2007;28:3153–62.
[13] Montalbetti CAGN, Falque V. Amide bond formation and peptide coupling. Tetrahedron 2005;61:10827–52.
[14] Nakajima N, Ikada Y. Mechanism of amide formation by carbodiimide for bioconjugation in aqueous media. Bioconj Chem 1995;6:123–30.
[15] Powell HM, Boyce ST. EDC cross-linking improves skin substitute strength and stability. Biomaterials 2006;34:5821–7.
[16] Buttafoco L, Engbers-Buijtenhuijs P, Poot AA, Dijkstra PJ, Vermes I, Feijen J. Physical characterization of vascular grafts cultured in a bioreactor. Biomaterials 2006;27:2380–9.
[17] Park S-N, Park J-C, Kim HO, Song MJ, Suh H. Characterization of porous collagen/hyaluronic acid scaffold modified by 1-ethyl-3-(3-dimethylaminopropyl)carbodiimide cross-linking. Biomaterials 2002;23:1205–12.
[18] Nam K, Kimura T, Kishida A. Controlling coupling reaction of EDC and NHS for preparation of collagen gels using ethanol/water co-solvents. Macro Biosci 2008;8:32–7.
[19] Nam K, Kimura T, Kishida A. Preparation and characterization of cross-linked collagen–phospholipid polymer hybrid gels. Biomaterials 2007;28:1–8.
[20] Petong P, Pottel R, Kaatze U. Dielectric relaxation of H-bonded liquids. Mixtures of ethanol and *n*-hexanol at different compositions and temperatures. J Phys Chem A 1999;103:6114–21.
[21] Bubnis WA, Ofner III CM. The determination of ε-amino groups in soluble and poorly soluble proteinaceous materials by a spectrophotometric method using trinitrobenzenesulfonic acid. Anal Biochem 1992;207:129–33.
[22] Everaerts F, Torrianni M, van Luyn M, van Wachem P, Feijen J, Hendriks M. Reduced calcification of bioprostheses, cross-linked via an improved carbodiimide based method. Biomaterials 2005;25:5523–30.
[23] Pieper JS, Hafmans T, Veerkamp JH, van Kuppevelt TH. Development of tailor-made collagen–glycosaminoglycan matrices: EDC/NHS crosslinking, and ultrastructural aspects. Biomaterials 2000;21:581–93.
[24] Pieper JS, Oosterhof A, Dijkstra PJ, Veerkamp JH, van Kuppevelt TH. Preparation and characterization of porous crosslinked collagenous matrices containing bioavailable chondroitin sulphate. Biomaterials 1999;20:847–58.
[25] Kiritoshi Y, Ishihara K. Molecular recognition of alcohol by volume phase transition of cross-linked poly(2-methacryloyloxyethyl phosphorylcholine) gel. Sci Tech Adv Mater 2003;4:93–8.
[26] Kiritoshi Y. Making phospholipid-type hydrogel for biomedical application with attention to cross-linking point. Ph.D. thesis, University of Tokyo; 2004 [chapter 4].
[27] Priel Z, Silberberg A. Conformation of poly(methacrylic acid) in alcohol–water mixtures. II. Methanol, ethanol, *n*-propanol, and 1,2-ethanediol. J Polym Sci A-2 1970;8:705–12.
[28] Sarmini K, Kenndler E. Capillary zone electrophoresis in mixed aqueous–organic media: effect of organic solvents on actual ionic mobilities, acidity constants and separation selectivity of substituted aromatic acids. II. Ethanol. J Chromatogr A 1998;811:201–9.
[29] Doğan A, Kılıç E. Tautomeric and microscopic protonation equilibria of some α-amino acids. Anal Biochem 2007;365:7–13.
[30] Ripamonti A, Roveri N, Briga D. Effects of pH and ionic strength on the structure of collagen fibrils. Biopolymers 1980;19:965–75.
[31] Rosenblatt J, Devereux B, Wallace D. Dynamic rheological studies of hydrophobic interactions in injectable collagen biomaterials. J Appl Polym Sci 1993;50:953–63.
[32] Russel AE, Cooper DR. Structural and functional factors in the hydrogen bonding of polar organic solvents to acid-soluble collagen. Effect on renaturation kinetics and thermal stability. Biochemistry 1969;8:3980–90.
[33] Bianchi E, Rampone A, Ciferri A. The role of aliphatic alcohols on the stability of collagen and tropocollagen. J Biol Chem 1970;245:3341–5.
[34] Usha R, Maheshwari R, Dhathathreyan A, Ramasami T. Structural influence of mono and polyhydric alcohols on the stabilization of collagen. Colloids Surf B 2006;48:101–5.

Acta Biomaterialia 6 (2010) 409–417

Contents lists available at ScienceDirect

Acta Biomaterialia

journal homepage: www.elsevier.com/locate/actabiomat

Preparation of a collagen/polymer hybrid gel for tissue membranes. Part II: In vitro and in vivo biological properties of the collagen gels

Kwangwoo Nam [a,b], Tsuyoshi Kimura [a,b], Seiichi Funamoto [a], Akio Kishida [a,b,*]

[a] Division of Biofunctional Molecules, Institute of Biomaterials and Bioengineering, Tokyo Medical and Dental University, 2-3-10 Kanda-Surugadai, Chiyoda-ku, Tokyo 101-0062, Japan
[b] JST-CREST, Honcho, Kawaguchi, Saitama 332-0012, Japan

ARTICLE INFO

Article history:
Received 5 January 2009
Received in revised form 11 May 2009
Accepted 11 June 2009
Available online 16 June 2009

Keywords:
Collagen
Phospholipid polymer
Inflammatory response
In vitro and in vivo studies

ABSTRACT

The aim of the present study was to evaluate the biological properties of a collagen–phospholipid polymer hybrid gel (MiC30 gel) designed for use as a tissue membrane. The following four types of collagen gels were synthesized and tested in vitro and in vivo: physically cross-linked collagen gel (Uc gel), *N*-(3-dimethylaminopropyl)-*N*′-ethylcarbodiimide (EDC)/*N*-hydroxysuccinimide-cross-linked collagen gel (EN gel), MiC30 gel and glutaraldehyde-cross-linked collagen gel (G gel). The cell adhesivity and proliferation rate were observed to be lowest for the MiC30 gel and highest for the Uc gel, indicating that the phospholipid–polymer-covered surface of the collagen gel interacted weakly with cells. The collagen gel was implanted into rats subcutaneously and was observed 1, 2 and 8 weeks after implantation. The Uc gel and G gel were degraded and induced an inflammatory response. Granulation was not observed for 8 weeks after implantation and the formation of foreign body giant cells was observed around both the Uc and G gels. On the other hand, cell infiltration and degradation were not observed in the case of the EN and MiC30 gels. The formation of foreign body giant cells was suppressed and the healing process was accelerated. The MiC30 gel is suitable for use as a biomaterial that is stable in vivo because it suppresses the foreign body response and accelerates the healing process.

1. Introduction

Commercially available collagens are used as scaffolding materials since collagen acts as a good extracellular matrix for the cell [1]. Collagen is mainly used for bone regeneration and the development of coating materials for vascular grafts or heart valves. Once the collagen product is implanted in the body it is degraded because of cell infiltration and is absorbed by the body. The speed of degradation is uncontrollable and differs depending on the physical properties of the collagen or the structure of the three-dimensional matrix formed by it. To solve this problem, cross-linking of collagen products was introduced.

Many researchers have cross-linked proteins or polypeptides using *N*-(3-dimethylaminopropyl)-*N*′-ethylcarbodiimide (EDC) as the cross-linker, since it brings about the formation of an amide linkage between a carboxyl group and an amine moiety [2–9]. Cross-linking using a polymer of this molecule has also been investigated, primarily to achieve synergic effects of the polymer and collagen, such as hemocompatibility or mechanical strength [10].

In the first phase of this study we developed a novel method for collagen–polymer cross-linking; we cross-linked collagen gel with a 2-methacryloyloxyethyl phosphorylcholine (MPC)-based copolymer, namely poly(MPC-co-methacrylic acid) (PMA), a well-known hemocompatible and anti-inflammatory polymer [11–14], in water/ethanol co-solvent to obtain a collagen/phospholipid polymer hybrid gel (MiC gel). We found that MiC30 gel, which had been cross-linked with MPC:MA = 30:70 (PMA30), and collagen showed the highest cross-linking rates when the molar concentration of ethanol (N_A) was approximately 0.12 (30 vol.% aqueous solution of ethanol). Denaturization of the collagen triple helix after cross-linking was not observed and the collagen gel remained dimensionally stable and transparent [15]. Its mechanical strength increased compared with that of uncross-linked collagen gel.

In the second phase of this study we investigated the in vitro and in vivo behavior of the collagen gel. We first compared the biological properties of collagen gels prepared in a 2-morpholinoethane sulfonic acid (MES) buffer and those prepared in an ethanol/water co-solvent in vitro. Then, we implanted the prepared collagen gels in vivo to characterize the reaction of the body to the collagen gels. For this study we chose PMA30 to prepare a collagen–phospholipid hybrid gel in a 30% aqueous solution of ethanol (MiC30 gel), since this gel contained a highest amount of MPC polymer among the collagen gels we had prepared. We tried to

* Corresponding author. Address: Division of Biofunctional Molecules, Institute of Biomaterials and Bioengineering, Tokyo Medical and Dental University, 2-3-10 Kanda-Surugadai, Chiyoda-ku, Tokyo 101-0062, Japan. Tel./fax: +81 03 5841 8028.
E-mail address: kishida.fm@tmd.ac.jp (A. Kishida).

1742-7061/$ - see front matter © 2009 Acta Materialia Inc. Published by Elsevier Ltd. All rights reserved.
doi:10.1016/j.actbio.2009.06.022

characterize the MiC30 gel by investigating how the body responds to the implanted material over time.

2. Materials and methods

2.1. Preparation of the collagen gels

2.1.1. Preparation of EDC and NHS-cross-linked collagen gel (EN gel)

An EDC and NHS-cross-linked collagen gel (EN gel) was prepared by a previously reported method [15,16]. A 2 wt.% collagen type I solution was prepared and used for film preparation instead of a 0.5 wt.% collagen type I aqueous solution (pH 3) (KOKEN, Tokyo, Japan). The collagen solution was added dropwise to polyethylene film and allowed to dry at room temperature. The collagen film (thickness 56 ± 3 μm) was immersed in a 30 vol.% aqueous solution of ethanol (N_A = 0.12) containing EDC (Kanto Chemicals, Tokyo, Japan) and *N*-hydroxysuccinimide (NHS) (Kanto Chemicals). The molar ratio of the constituents, i.e. EDC, NHS and the collagen carboxylic acid groups, was 10:10:1. The cross-linking process was allowed to proceed at 4 °C for 24 h to yield a cross-linked gel (EN gel). After 24 h the reaction was terminated by removing the gel from the solution. Subsequently the gel was first washed with a 4 M aqueous solution of Na_2HPO_4 for 2 h to hydrolyze any remaining *O*-acylisourea groups and then with distilled water for at least 3 days to remove traces of salts from the gel.

2.1.2. Preparation of the collagen/phospholipid hybrid gel

PMA was synthesized using a previously reported method [16,17]. MPC and methacrylic acid (MA) were co-polymerized in ethanol solution for 16 h at 60 °C using 2,2-azobisisobutyronitrile as an initiator. The molar ratio of MPC to MA was 3:7 in PMA30 and 9:1 in PMA90; the number average molecular weight of PMA was 3×10^5.

A 2 wt.% collagen type I solution was prepared and film preparation was carried out using the same film that was developed for EN gel preparation. MiC30 gel was prepared using collagen film. PMA30 was added to a 30% aqueous solution of ethanol (N_A = 0.12) along with EDC and NHS. The polymer was activated for 10 min before the collagen film was immersed in the above mentioned solution. The molar proportions of each chemical were fixed; EDC, NHS and collagen carboxylic acid groups were present in the ratio 10:10:1. The cross-linking of PMA with collagen was continued for 24 h at 4 °C to yield the MiC30 gel.

2.1.3. Preparation of glutaraldehyde-cross-linked collagen gel

Collagen gel was cross-linked with glutaraldehyde by a previously reported method [18]. In brief, a 25% glutaraldehyde solution (Merck, Damstadt, Germany) was diluted to 0.5 wt.% in phosphate-buffered saline (PBS). The collagen film was immersed in the glutaraldehyde/PBS solution and the cross-linking process was allowed to proceed for 3 h at room temperature. After cross-linking the sample was first rinsed in running tap water for 30 min and then in 0.5 M NaCl for 2 h. In order to remove NaCl, the sample was rinsed with distilled water for 1 day to obtain a glutaraldehyde-cross-linked collagen gel (G gel). The biological properties of this gel were compared with those of the MiC30 gel.

A collagen film stabilized in MES buffer, pH 9.0 (Uc gel) for 24 h was prepared for use as a control for in vitro and in vivo studies.

2.2. Biological characterization of collagen gels

2.2.1. Cell adhesion test in vitro

The interaction between L929 cells (mouse fibroblasts) and the collagen gels was investigated in vitro. The collagen gels (radius 0.5 cm) were sterilized by placing the gels first in a 50:50 ethanol/water solution for 2 h, then in a 70:30 ethanol/water solution for 2 h and, finally, in a 100:0 ethanol/water solution overnight. Subsequently the gels were lyophilized. The lyophilized gels were hydrolyzed with Eagle's minimum essential medium (E-MEM) (Gibco, NY) for 30 min in a 48-well plate placed on a clean bench. The E-MEM was discarded just before cell seeding. The fibroblasts were cultured in E-MEM supplemented with 10% fetal bovine serum (FBS) (Gibco at 37 °C in a 5% CO_2 atmosphere. After treatment with 0.25% trypsin the cell density was adjusted to 5×10^3 cells ml^{-1} and the cells were seeded on the gel surface. After 24 and 48 h cycles the number of cells adhering to the gels was measured using a UV/visual spectrophotometer (V-560; Jasco, Tokyo, Japan) at 560 nm by performing a lactate dehydrogenase (LDH) assay (Wako Chemicals, Tokyo, Japan) [13,16]. All experiments were repeated five times and the values are expressed as means ± standard deviations. Statistical analysis was performed using the ANOVA test, with the significance at $P < 0.05$.

Cell viability and morphology were investigated in a standard medium containing 2-μM calcein acetoxymethylester (calcein-AM, Dojindo, Kumamoto, Japan). The viability of L929 cells containing calcein-AM was evaluated for cells grown for 24 h. The cells were observed under a fluorescent microscope (TE 2000-U, Nikon, Tokyo, Japan) with a 488 nm filter. The hydrolyzed dye (calcein-AM) emits a green fluorescence, which indicates cell viability.

2.2.2. Implantation and histological procedure

The animal study was performed in accordance with the NIH guidelines for the care and use of laboratory animals (NIH Publication 85-23, revised 1985) and the Tokyo Medical and Dental University guidelines. Wistar rats (7 weeks old, male, 250 g) were divided into four experimental groups. Each group was studied at 1, 2 and 8 weeks from the beginning of the experiment. After the animals were anesthetized with diethyl ether (Kanto Chemicals they were shaved and disinfected with 70% ethanol. Then, four different incisions (~1.5–2 cm) were made on the backs of the rats. Uc gel, EN gel, MiC30 gel and G gel (radius 0.5 cm) was implanted subcutaneously into the incision sites (n = 6), which were then immediately sewn up. Each rat was implanted with four different kinds of samples on its back. After 1, 2 and 8 weeks the rats were killed with an overdose of ethyl ether. The rat tissue containing the samples was excised from the rats and stained with hematoxylin and eosin (H–E). To study the inflammatory response, anti-rat macrophage/dendritic cell monoclonal antibodies (RM-4, Trans Genic Inc., Kumamoto, Japan) were used [19]. Rat spleen was used as the positive and negative control. The sample preparation and staining procedures used were the same as those used by technicians in the Applied Medical Research Laboratory (Osaka, Japan).

3. Results

3.1. In vitro results

Fig. 1 shows cell adhesivity to the surfaces of the collagen gels. Cell adhesion was the same in the case of the EN gel prepared in MES buffer and that prepared with an ethanol/water co-solvent. However, cell adhesion and proliferation decreased when the MiC30 gel was prepared in an ethanol/water co-solvent. The lowest rate of cell adhesion was observed in the case of the G gel. We could not find proof that high intra- and interhelical cross-linking decreases or increases cell adhesion once the free amine group content is lower than 70% (data not shown).

The cells that adhered were viable after 24 h incubation, as shown in Fig. 2. Since the collagen gels were transparent (with the exception of the G gel, which was light yellow), a clear fluorescence image could be obtained. The cells on tissue culture polystry-

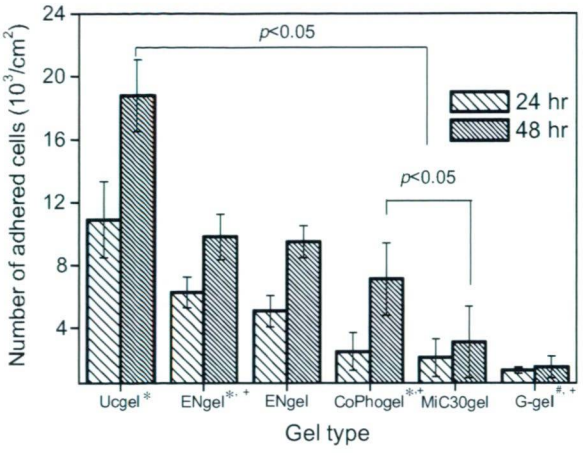

Fig. 1. Cell adhesion property of the respective collagen gels at a seeding density of 5000 cells cm^{-2}. Each value represents the mean ± SD (n = 5). *Prepared in MES buffer (alkaline pH). #Prepared in PBS solution. +Ref. [16].

rene (TCPS), Uc gel and EN gel showed deformations, while the cells on the MiC30 gel had a round morphology. This agrees with the data previously presented by Watanabe et al. [13], who mentioned that the deformations occurred because of a weak interaction between the cell and the gel surface.

3.2. In vivo results

Figs. 3 and 4 show the histological results obtained 2 weeks after implantation. The Uc gel showed extensive degradation, while the G gel showed slight degradation. The EN and MiC30 gels remained stable. A wide distribution of macrophages could be observed around all except the MiC30 gel, which shows that macrophages were concentrated on the surface of the MiC30 gel. RM staining revealed classic encapsulation around the G gel, with the formation of a large number of foreign body giant cells, as seen in Fig. 4d. The results revealed that macrophages were very active 2 weeks after implantation. The darkly stained cells were obviously macrophages, since RM-4 can only stain macrophages and dendritic cells [19]. Furthermore, the debris resulting from degradation of the gel could be seen. Macrophage fusion was not induced on other collagen gels. A comparison of the tissue response around the EN and MiC30 gels revealed that the number of lymphocytes and macrophages around the EN gel was greater than around the MiC30 gel. The granulation process had already begun in the MiC30 gel.

Figs. 5 and 6 show the histological results obtained after 8 weeks implantation. In five of the six cases where the Uc gel was implanted the gel was completely degraded 8 weeks after implantation. The tissue was completely infiltrated by lymphocytes, macrophages and foreign body giant cells. Degradation of the G gel was still in progress and debris from the G gel was visible. Foreign body giant cells were also observed in this case. In the case of both the Uc and G gels no granulation was observed, as indicated by the absence of fibroblasts or newly formed collagen. Granulation tissue was clearly visible around the EN and MiC30 gels, with a small number of lymphocytes and macrophages. Both the EN and MiC30 gels showed biostability in vivo. The thickness of the new collagen layer was much greater at 8 weeks after implantation than at 2 weeks after implantation. The most mature collagen layer was seen in the tissue implanted with the MiC30 gel, while the tissue implanted with the EN gel showed a thin collagen layer. Neovascularization was observed in all sample tissues except for those implanted with the MiC30 gel. A brown layer, which is thought to be stained by EnVison™, was observed for all samples.

4. Discussion

4.1. Cell–matrix interaction in vitro

The MPC polymer is known to be bioinert in vitro and in vivo [11–16]. The best explanation for this fact is based on free water theory [11]. The free water present around the MPC polymer prevents protein adsorption and cell adhesion [20,21]. Cell death due to inability of the cell to attach itself to the MPC surface would not occur because the MPC head group interacts weakly with the cell. Cross-linking of the MPC polymer and collagen gel prevents

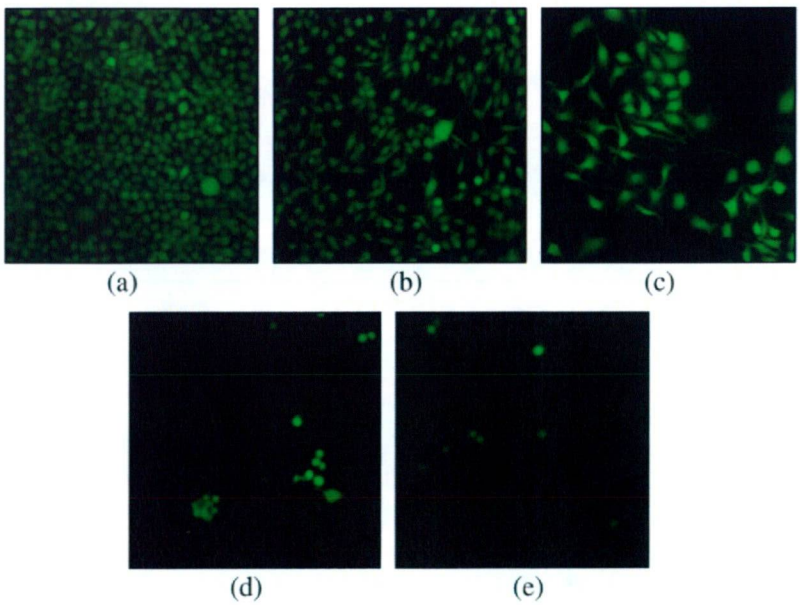

Fig. 2. Fluorescence images of cells adhering to the collagen gels. (a) TCPS; (b) Uc gel; (c) EN gel; (d) MiC30 gel; and (e) G gel. Magnification 2×.

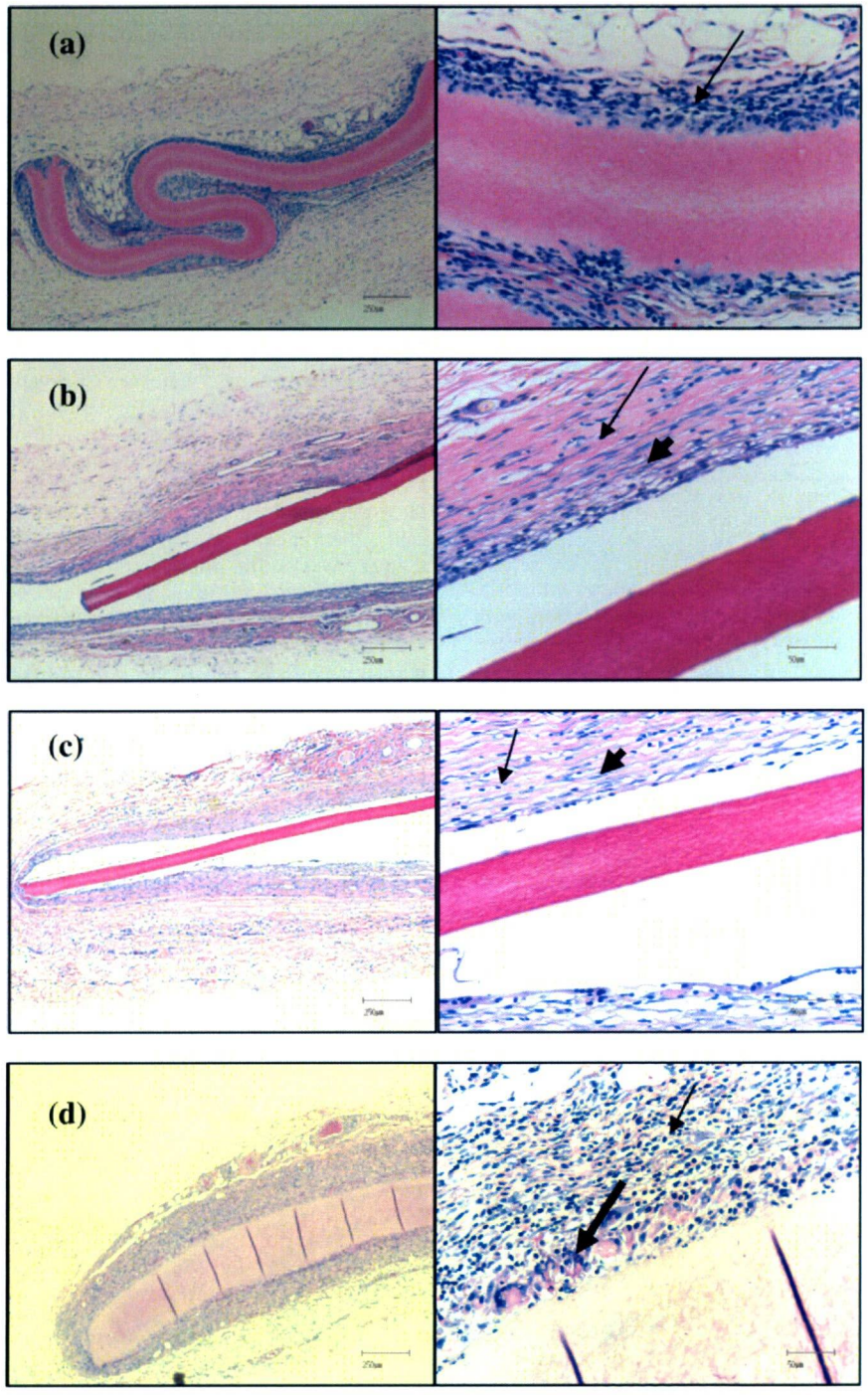

Fig. 3. H–E stained histological images of the respective collagen gels after 2 weeks implantation. The images on the left are shown at a magnification of 4× and those on the left are shown at a magnification of 20×. The long thick arrow indicates a foreign body giant cell, the long thin arrow indicates lymphocytes and the short thick arrow indicates a fibroblast.

collagenase activation in vitro [15], suggesting that the MiC30 gel would be biostable in vivo.

In vitro experiments showed that cell adhesion and cell proliferation were suppressed in the case of the MiC30 gel (Fig. 1); this suppression is even more evident when these experimental results are compared with the cell adhesivity of a CoPho gel prepared in MES buffer. The greater suppression in the case of the MiC30 gel is due to an increase in the number of MPC moieties caused by the higher cross-linking rate [13]. The increase in the intra- and interhelical collagen network did not alter the cell adhesion properties significantly. After 24 and 48 h the cell adhesivity of the EN gel prepared in MES buffer did not differ significantly from that of the EN gel prepared in an ethanol/water co-solvent. This implies that the suppression of cell adhesion and cell proliferation is solely due to the increase in the number of MPC moieties, which makes the surface of the collagen gel inert.

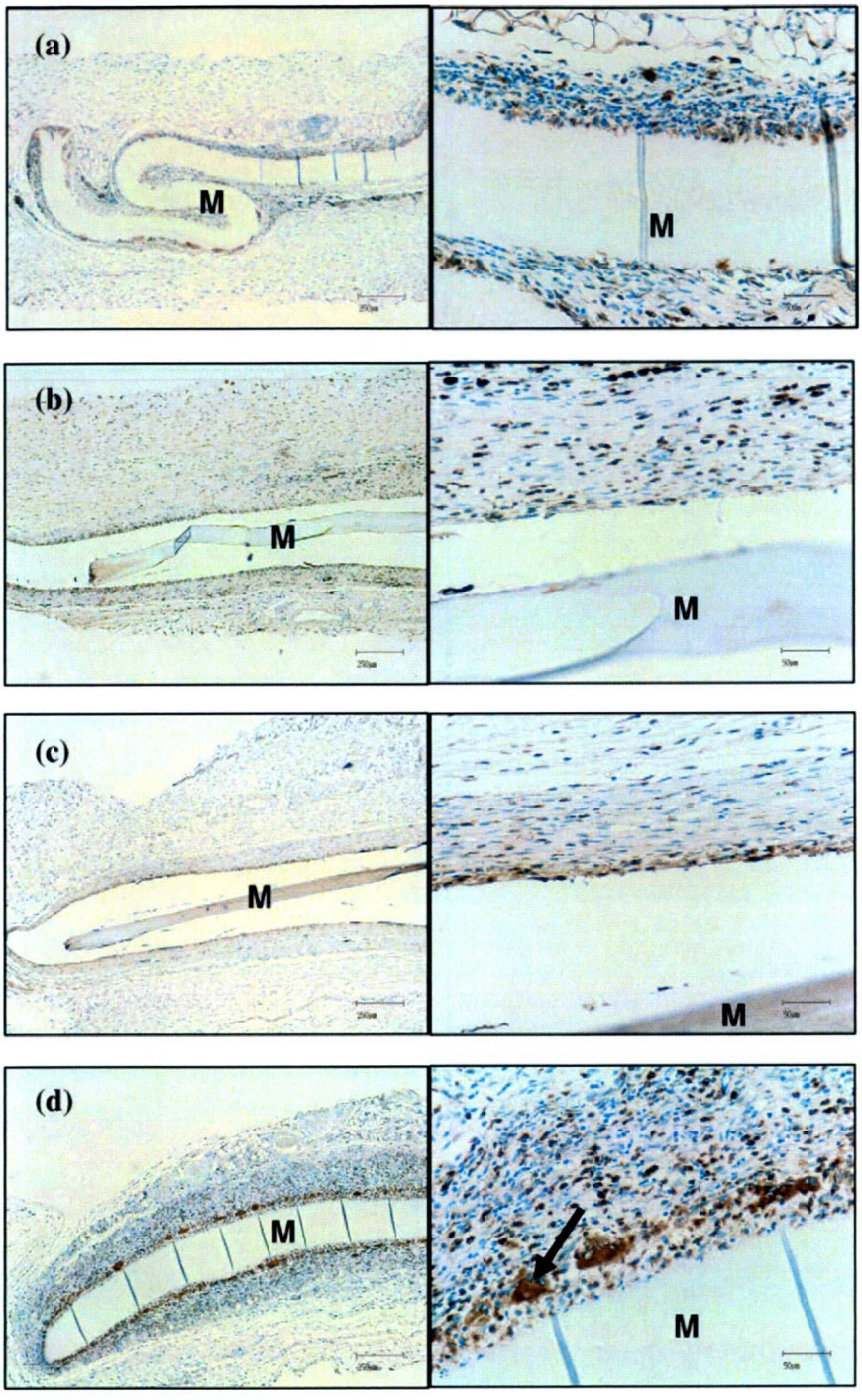

Fig. 4. RM-4 stained histological images of the respective collagen gels after 2 weeks implantation. The images on the left are shown at a magnification of 4× and those on the left are shown at a magnification of 20×. Macrophagea are shown in black. The foreign body giant cell is indicated by a thick arrow. The letter M indicates the matrix.

4.2. Wound healing response of the body in vivo

As is evident from Figs. 3–6, classical encapsulation was observed only in the tissue implanted with G gel. Foreign body giant cells were clearly visible 2 weeks after implantation (Figs. 3 and 4). In the case of the Uc gel the acute inflammatory response almost disappeared 1 week after implantation and appeared to be changing to a chronic inflammatory response (Supplementary Figs. 1 and 2). At this point red blood cells were seen, but neutrophils and monocytes were not visible. Cell infiltration began 1 week after implantation; degradation began at the end of 2 weeks; complete degradation was seen 8 weeks after implantation. Macrophage fusion was seen 8 weeks after implantation, indicating that a chronic inflammatory response continued throughout this period. This is thought to be due to the effect of the native collagen structure, where the telopeptide has remained in the Uc gel.

For the G gel, slow degradation was clearly observed 8 weeks after implantation (Fig. 6d). It is known that inflammation can be

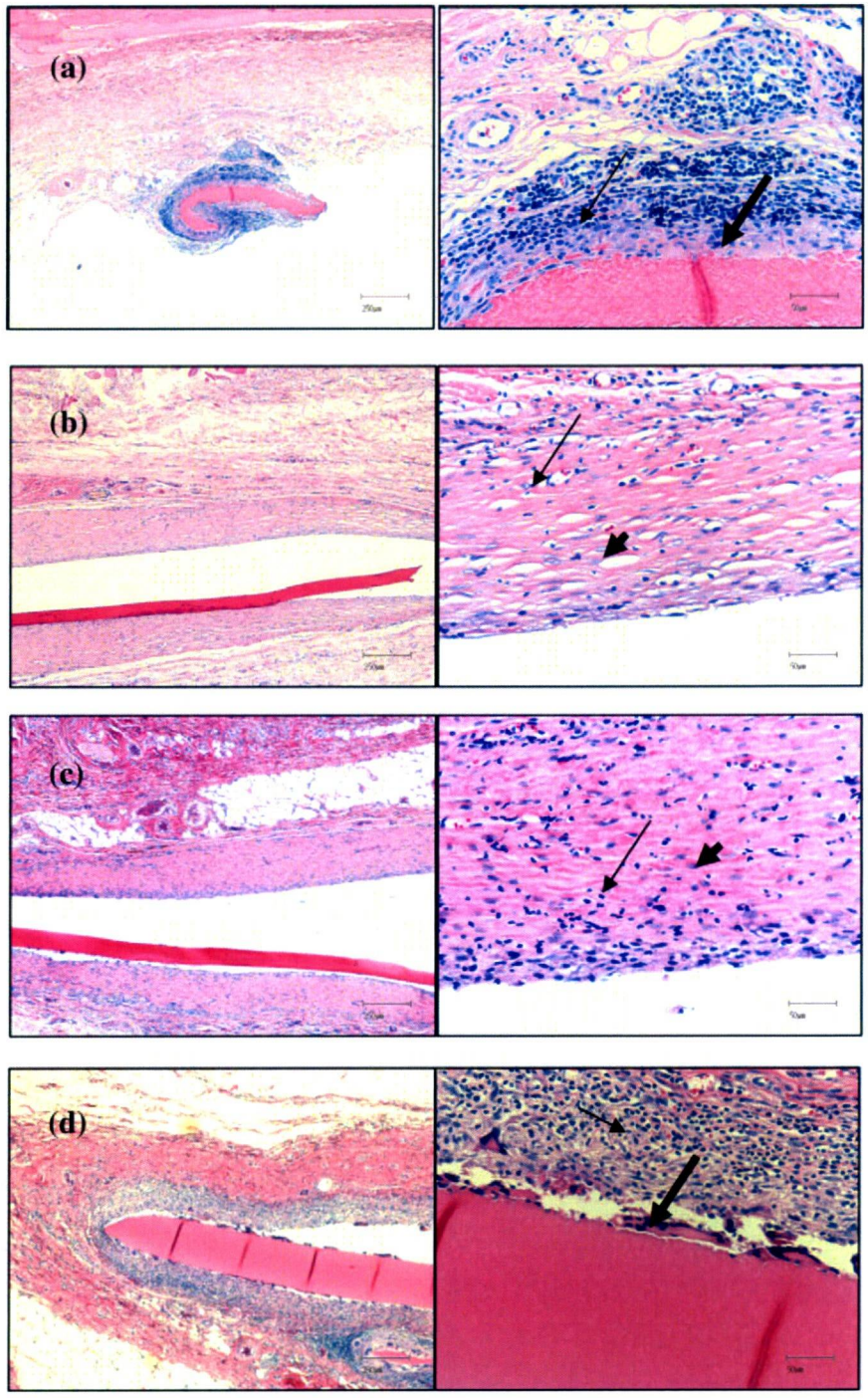

Fig. 5. H–E stained histological images of the respective collagen gels after 8 weeks implantation. The images on the left are shown at a magnification of 4× and those on the left are shown at a magnification of 20×. The long thick arrow indicates a foreign body giant cell, the long thin arrow indicates lymphocytes and the short thick arrow indicates a fibroblast.

suppressed when the concentration of glutaraldehyde used is less than 0.01 wt.% [22]. However, in this case a high inflammatory response was observed, since the G gel was prepared using 0.25 wt.% glutaraldehyde. This conclusion is confirmed by the work of van Wachem et al. [23]. Debris from the gel and macrophage fusion around the debris demonstrated the typical failure of artificial biomaterials [24]. On the basis of these observations it can be inferred that glutaraldehyde leaked into the G gel during degradation and triggered activation of macrophage fusion by binding with interleukin, which induces the formation of foreign body giant cells [25,26]. Neither fibroblasts nor a new collagen layer was formed around either the Uc gel or G gel, indicating that the chronic inflammatory response would continue 8 weeks after implantation (Fig. 5a and d).

On the other hand, the EN and MiC30 gels did not show any degradation. One week after implantation an acute inflammatory

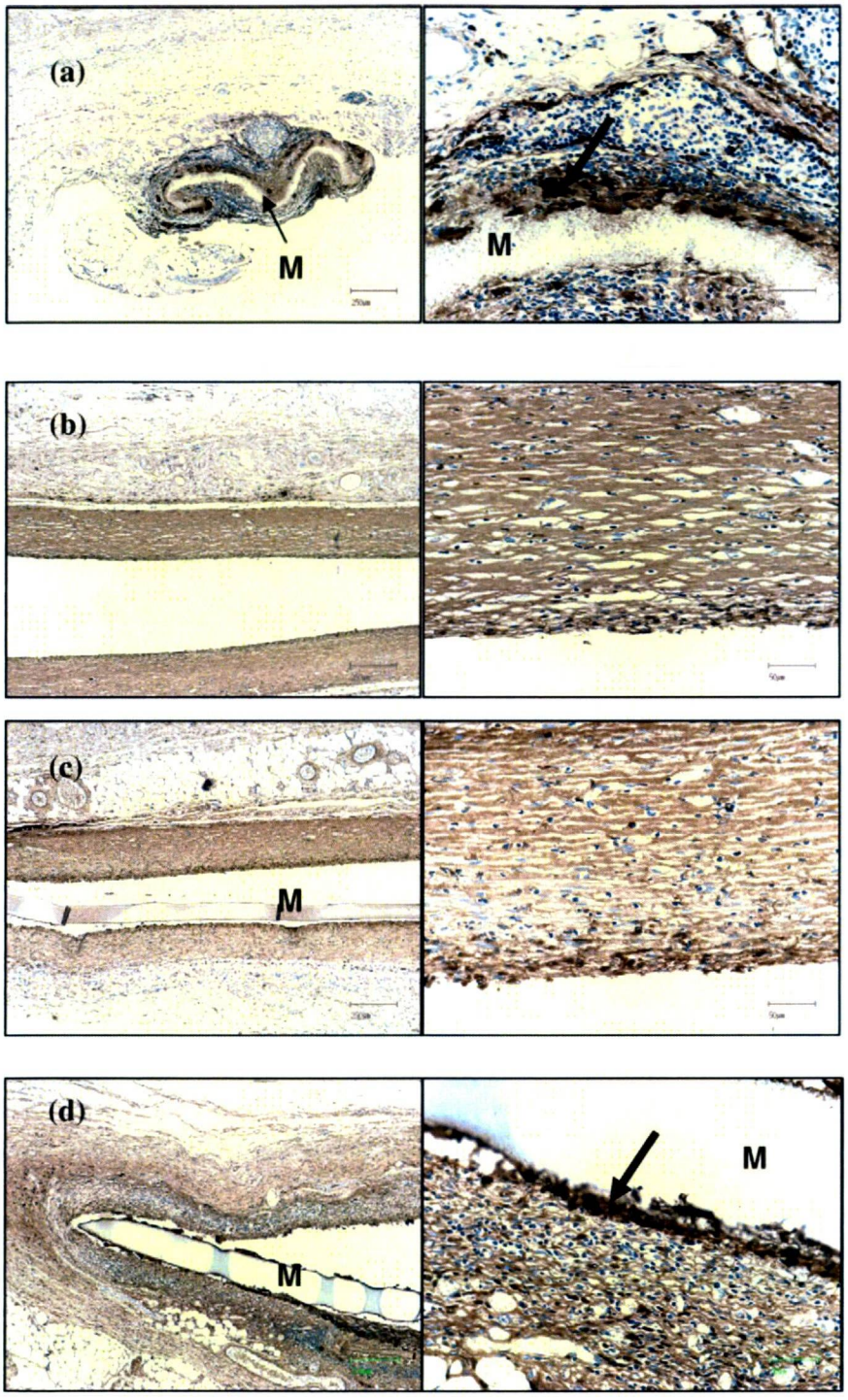

Fig. 6. RM-4 stained histological images of the respective collagen gels after 8 weeks implantation. The images on the left are shown at a magnification of 4× and the on the left are shown at a magnification of 20×. Macrophages are shown in black. The foreign body giant cell is indicated by a thick arrow. The letter M indicates the matrix.

response and blood clots were observed, while 2 weeks after implantation fibroblasts were seen and the formation of a new collagen layer could be observed (Fig. 3). This implies that granulation, which is the final stage of wound healing, had already begun [27]. In the case of the EN gel the macrophages were distributed over a large area in the newly formed tissue, while in the case of the MiC30 gel the macrophages were concentrated on the surface of the cell–matrix (Fig. 4c). No wide macrophage distribution was observed, suggesting that by this time the tissue surrounding the MiC30 gel is in the process of granulation. The wide distribution of macrophages and lymphocytes in the tissue implanted with the EN gel indicates the induction of a response to the foreign body [28]. This is because lymphocytes associate with macrophages. However, foreign body giant cells were not observed following EN gel implantation.

The formation of foreign body giant cells is caused by macrophage fusion, which occurs due to two factors: phagocytosis and the prevention of anoikis [25,29–31]. Both factors rely on cell–ma-

trix interaction; a lesser extent of cell adhesion to the matrix leads to macrophage fusion [25]. This is generally observed for artificial biomaterials. It is interesting to note that collagen gels cross-linked with glutaraldehyde alone behave similarly to artificial biomaterials. The weak cell–matrix interaction observed in vitro (Fig. 2e) resulted in the formation of a large number of foreign body giant cells. In the case of the EN gel cross-linking at carboxyl groups by amide formation renders cell attachment difficult [16,32,33]. The strong cross-links also prevent degradation of the gels by collagenase.

It should be noted that the surfaces of the EN and MiC30 gels were not completely inert. As seen in Fig. 2c and d, cells attached themselves to the surface of the matrix. The morphology of the attached cells suggests that there was a slight cell–matrix interaction. Previous studies [16], as well as Figs. 1 and 2, suggest that protein adsorption was not completely suppressed. Therefore, a slight cell–matrix interaction may still occur, which may lead to the prevention of the macrophage fusion. The cell–matrix interactions in the case of the EN and G gels were different. Furthermore, in the EN gel the cross-linking involved carboxyl groups, while the G gel consisted of amine–amine cross-links [10]. Carboxyl groups are known to enhance cell attachment and contribute to macrophage fusion on the surface of the matrix [32–34]. Moreover, intra- and interhelical cross-links make the EN gel stable against collagenase activity [15]. Thus, the factors that contributed to the suppression of macrophage fusion and encapsulation are as follows: lack of available carboxyl groups, slight cell–matrix interaction and stability against collagenase activity. Similar findings were reported by Wissink [35]. In the case of the MiC30 gel the suppression of macrophage fusion and encapsulation are thought to have occurred because of the existence of the MPC moiety, which suppressed protein adsorption. By 8 weeks after implantation lymphocytes and macrophages disappeared from sites implanted with the EN gel (Fig. 6b).

Eight weeks after MiC30 gel implantation the new collagen layer that formed was very thick and, hence, it stabilized the gel; almost no macrophages were detected in the collagen layer. On the other hand, for the EN gel the newly formed collagen layer was still thin at 8 weeks. Foreign body giant cells were not present on the surface of MiC30 gels, since the MPC moiety does not adsorb interleukin [12,36]. No foreign body giant cells were formed around the EN and MiC30 gels, but the distribution of lymphocytes and macrophages was different in the two cases. The absence of foreign body giant cells indicates that the foreign body response was not triggered [25,28]. This can be explained by the hydrophilic nature of the MPC moiety [16,37], such that the body did not recognize the MiC30 gel as a foreign substance.

This difference in thickness of the newly formed collagen layer can be attributed to the presence of the MPC moiety in the MiC30 gel and EN gel, suggesting that the healing process was fastest in the case of tissue implanted with the MiC30 gel. As mentioned above, a wide macrophage distribution was seen in the case of EN gel implantation. This can be explained by the fact that macrophages are also involved in the regulation of fibrous proliferation and neovascularization [38] Two weeks after EN gel implantation lymphocytes, fibroblasts and macrophages were seen, but 8 weeks after implantation most of the cells were fibroblast cells. As mentioned above, granulation was slower around the EN gel than around the MiC30 gel and, hence, macrophage activation was observed 2 and 8 weeks after implantation. Further, neovascularization was clearly seen 8 weeks after implantation (Fig. 5b), supporting the fact that macrophages were active.

5. Conclusion

In this study, we have tried to establish the mechanism of cross-linking of collagen gels using EDC and NHS and synthesize a polymer–collagen hybrid gel that can be used as a tissue membrane. Our results indicate that the MiC30 gel is not recognized by the body as a foreign substance, and this result in suppression of encapsulation and an increase in the wound healing rate. Furthermore, no cracking or leaking of polymer was observed. The absence of macrophage fusion also implies that cell death is controlled; this, in turn, implies that the MPC polymer is non-toxic.

In conclusion, we would like to state that this MiC30 gel is a novel biomaterial that is stable in vivo and can be used in clinical applications such as tissue membranes. This gel can remain inert in the tissue for a long time, stay positioned in the implanted site and suppress undesired inflammatory responses of the body.

Acknowledgements

This work was supported in part by Grants-in-Aid from Research on Health Sciences focusing on Drug Innovation from the Japan Health Sciences Foundation and Research on the Human Genome, Tissue Engineering, Health and Labour Science Research Grant, Ministry of Health, Labour and Welfare, Japan. This work was also partly supported by a Grant-in-Aid from the Core Research for Evolutional Science and Technology (CREST) of the Japan Science and Technology Agency (JST). We would like to thank Professor Kazuhiko Ishihara of the University of Tokyo for his kind assistance and advice on the preparation and analysis of the MPC polymer.

Appendix A. Figures with essential colour discrimination

Certain figures in this article, particularly Figs. 2–6, are difficult to interpret in black and white. The full colour images can be found in the on-line version, at doi: 10.1016/j.actbio.2009.06.022.

Appendix B. Supplementary data

Supplementary data associated with this article can be found, in the online version, at doi:10.1016/j.actbio.2009.06.022.

References

[1] Schor AM, Schor SL, Kumar S. Importance of a collagen substratum for stimulation of capillary endothelial cell proliferation by tumor angiogenesis factor. Int J Cancer 1979;24:225–34.
[2] van Luyn MJA, van Wachem PB, Olde Damink LHH, Dijkstra PJ, Feijen J. Relations between in vitro cytotoxicity and crosslinked dermal sheep collagens. J Biomed Mater Res 1992;26:1091–110.
[3] Olde Damink LHH, Dijkstra PJ, van Luyn MJA, van Wachem PB, Nieuwenhuis P, Feijen J. Crosslinking of dermal sheep collagen using a water-soluble carbodiimide. Biomaterials 1996;17:765–73.
[4] van Wachem PB, Zeeman R, Dijkstra PJ, Feijen J, Hendriks M, Cahalan PT, et al. Characterization and biocompatibility of epoxy-crosslinked dermal sheep collagens. J Biomed Mater Res 1999;47:270–7.
[5] Gratzer PF, Lee JM. Control of pH alters the type of cross-linking produced by 1-ethyl-3-(3-dimethylaminopropyl)-carbodiimide (EDC) treatment of acellular matrix vascular grafts. J Biomed Mater Res 2001;58:172–9.
[6] Wissink MJB, Beernink R, Pieper JS, Poot AA, Engbers GHM, Beugeling T, et al. Immobilization of heparin to EDC/NHS-crosslinked collagen, characterization and in vitro evaluation. Biomaterials 2001;22:151–63.
[7] Everaerts F, Torrianni M, van Luyn M, van Wachem P, Feijen J, Hendriks M. Reduced calcification of bioprostheses, cross-linked via an improved carbodiimide based method. Biomaterials 2005;25:5523–30.
[8] Liu L, Kuffová L, Griffith M, Dang Z, Muckersie E, Liu Y, et al. Immunological responses in mice to full-thickness corneal grafts engineered from porcine collagen. Biomaterials 2007;28:3807–14.
[9] Marzec E, Pietrucha K. The effect of different methods of cross-linking of collagen on its dielectric properties. Biophys Chem 2008;132:89–96.
[10] Nimni ME, Cheung D, Strates B, Kodama M, Sheikh K. Chemically modified collagen: a natural biomaterial for tissue replacement. J Biomed Mater Res 1987;21:741–71.
[11] Ishihara K, Nomura H, Mihara T, Kurita K, Iwasaki Y, Nakabayashi N. Why do phospholipid polymers reduce protein adsorption? J Biomed Mater Res 1998;39:323–30.
[12] Iwasaki Y, Sawada S, Ishihara K, Khang G, Lee HB. Reduction of surface-induced inflammatory reaction on PLGA/MPC polymer blend. Biomaterials 2002;23:3897–903.

[13] Watanabe J, Ishihara K. Phosphorylcholine and poly(D,L-lactic acid) containing copolymers as substrate for cell adhesion. Artif Organs 2003;27:242–8.
[14] Ye SH, Watanabe J, Takai M, Iwasaki Y, Ishihara K. High functional hollow fiber membrane modified with phospholipid polymers for a liver assist bioreactor. Biomaterials 2006;27:1955–62.
[15] Nam K, Kimura T, Kishida A. Controlling coupling reaction of EDC and NHS for preparation of collagen gels using ethanol/water co-solvents. Macro Biosci 2008;8:32–7.
[16] Nam K, Kimura T, Kishida A. Physical and biological properties of collagen–phospholipid polymer hybrid gels. Biomaterials 2007;28:3153–62.
[17] Nam K, Kimura T, Kishida A. Preparation and characterization of cross-linked collagen–phospholipid polymer hybrid gels. Biomaterials 2007;28:1–8.
[18] Olde Damink LH, Dijkstra PJ, Van Luyn MJ, Van Wachem PB, Nieuwenhuis P, Feijen J. Changes in the mechanical properties of dermal sheep collagen during in vitro degradation. J Biomed Mater Res 1995;29:139–47.
[19] Iyonaga K, Takeya M, Yamamoto T, Ando M, Takahashi K. A novel monoclonal antibody, RM-4, specifically recognizes rat macrophages and dendritic cells in formalin-fixed, paraffin-embedded tissues. Histochem J 1997;29:105–16.
[20] Nam KW, Watanabe J, Ishihara K. Characterization of the spontaneously forming hydrogels composed of water-soluble phospholipid polymers. Biomacromolecules 2002;3:100–5.
[21] Morisaku T, Watanabe J, Konno T, Takai M, Ishihara K. Hydration of phosphorylcholine groups attached to highly swollen polymer hydrogels studied by thermal analysis. Polymer 2008;49:4652–7.
[22] McPherson JM, Sawamura S, Armstrong R. An examination of the biologic response to injectable, glutaraldehyde cross-linked collagen implants. J Biomed Mater Res 1987;20:93–107.
[23] van Wachem PB, van Lyun MJA, Olde Damink LHH, Dijkstra PJ, Feijen J, Nieuwenhuis P. Biocompatibility and tissue regenerating capacity of crosslinked dermal sheep collagen. J Biomed Mater Res 1987;28:353–63.
[24] Kao WJ, Zhao QH, Hiltner A, Anderson JM. Theoretical analysis of in vivo macrophage adhesion and foreign body giant cell formation on polydimethylsiloxane, low density polyethylene, and polyetherurethanes. J Biomed Mater Res 1994;28:73–9.
[25] Anderson JM, Rodriguez A, Chang DT. Foreign body reaction to biomaterials. Seminar Immunol. 2008;20:86–100.
[26] Jones JA, Dadsetan M, Collier TO, Ebert M, Stokes KS, Ward RS, et al. Macrophage behavior on surface-modified polyurethanes. J Biomater Sci Polym Ed 2004;15:567–84.
[27] Strodtbeck F. Physiology of would healing. Newborn Infant Nurs Rev 2001;1:43–52.
[28] Brodbeck WG, Macewan M, Colton E, Meyerson H, Anderson JM. Lymphocytes and the foreign body response: lymphocyte enhancement of macrophage adhesion and fusion. J Biomed Mater Res A 2005;74:222–9.
[29] Brodbeck WG, Shive MS, Colton E, Nakayama Y, Matsuda T, Anderson JM. Influence of biomaterial surface chemistry on the apoptosis of adherent cells. J Biomed Mater Res 2001;55:661–8.
[30] Ratner BD. Reducing capsular thickness and enhancing angiogenesis around implant drug release systems. J Controlled Release 2002;78:211–8.
[31] Redding PJ, Juliano RL. Clinging to life: cell to matrix adhesion and cell survival. Cancer Metastasis Rev 2005;24:425–39.
[32] Ber S, Köse T, Hasırcı V. Bone tissue engineering on patterned collagen films: an in vitro study. Biomaterials 2005;26:1977–86.
[33] Chandy T, Das GS, Wilson RF, Rao GHR. Use of plasma glow for surface-engineering biomolecules to enhance blood compatibility of Dacron and PTFE vascular prosthesis. Biomaterials 2000;21:699–712.
[34] Nair A, Zou L, Bhattacharyya L, Timmons RB, Tang L. Species and density of implant surface chemistry affect the extent of foreign body reactions. Langmuir 2008;24:2015–24.
[35] Wissink MJB. Endothelialization of collagen matrices. Doctoral thesis, University of Twente; 1999. p. 159–79 [chapter 8].
[36] Chiba N, Ueda M, Shimada T, Jinno H, Watanabe J, Ishihara K, et al. Novel immunosuppressant agents targeting activated lymphocytes by biocompatible MPC polymer conjugated with interleukin-2. Eur Surg Res 2007;39:103–10.
[37] Xu LC, Siedlecki CA. Effects of surface wettability and contact time on protein adhesion to biomaterial surfaces. Biomaterials 2007;28:3273–83.
[38] Martin P, Leibovich SJ. Inflammatory cells during wound repair: the good, the bad, and the ugly. Trends Cell Biol 2005;15:599–607.

Biomaterials 31 (2010) 3590–3595

Contents lists available at ScienceDirect

Biomaterials

journal homepage: www.elsevier.com/locate/biomaterials

The use of high-hydrostatic pressure treatment to decellularize blood vessels

Seiichi Funamoto [a,b], Kwangwoo Nam [a,b], Tsuyoshi Kimura [a,b], Ayako Murakoshi [a], Yoshihide Hashimoto [a,c], Kazuo Niwaya [d], Soichiro Kitamura [d], Toshiya Fujisato [d,e,**], Akio Kishida [a,b,*]

[a] Division of Biofunctional Molecules, Institute of Biomaterials and Bioengineering, Tokyo Medical and Dental University, 2-3-10, Kanda-surugadai, Chiyoda-ku, Tokyo 101-0062, Japan
[b] Japan Science and Technology Agency CREST, Japan 4-1-8, Honmachi, Kawaguchi, Saitama 332-0012, Japan
[c] Japan Society for the Promotion of Science, 5-3-1, Kojimachi, Chiyoda-ku, Tokyo 102-8471, Japan
[d] National Cardiovascular Center, 5-7-1, Fujishirodai, Suita, Osaka 565-8565, Japan
[e] Department of Biomedical Engineering, Osaka Institute of Technology, 5-16-1, Omiya, Asahi-ku, Osaka 535-8585, Japan

ARTICLE INFO

Article history:
Received 16 December 2009
Accepted 13 January 2010
Available online 9 February 2010

Keywords:
Arterial tissue engineering
Vascular graft
Mechanical property
Transplantation

ABSTRACT

A decellularization method using high-hydrostatic pressure (HHP) technology (>600 MPa) is described. The HHP disrupts the cells inside the tissue. The cell debris can be eliminated with a simple washing process, producing clean, decellularized tissue. In this study, porcine aortic blood vessel was decellularized by HHP. The mechanical properties and in vivo performance of the decellularized tissue were evaluated. Mechanical properties of the decellularized tissue were not altered by the HHP treatment. Reduced inflammation of the decellularized tissue was confirmed by xenogenic transplant experimentation. An allogenic transplantation study showed that decellularized blood vessel endured the arterial blood pressure, and there was no clot formation on the luminal surface. In addition, cellular infiltration into the vessel wall was observed 4 weeks after implantation, suggesting that HHP treatments could be applied widely as a high-quality decellularization method.

1. Introduction

Tissue engineering is one of the key technologies for treatment of atherosclerotic vascular diseases, valvular heart disease, aneurysm, and varices [1–4]. Decellularized tissue is promising as an ideal scaffold for cardiovascular tissue engineering. Several technologies have been developed to fabricate artificial valves and some of them have already been used clinically [5–7]. Decellularization techniques are classified by the chemicals used, such as acid or alkaline treatment, detergent treatment, or enzymatic digestion, and the physical methods used, such as snap freezing and mechanical agitation [8–12]. Among these, detergent treatment is the most widely used. Decellularization of biological tissues by detergent treatment has the advantage of being easy to use, but its drawbacks include long treatment time, alteration of mechanical properties, and residual toxicity [13]. Researchers have developed specific treatment recipes to overcome each of these problems.

As another candidate for a new decellularization treatment, we have reported our work on the high-hydrostatic pressure (HHP) method [14,15]. The unique characteristics of the HHP method are the destruction of cell membranes, uniform treatment, and short treatment time. Subsequent washing of the treated tissue can produce a decellularized tissue that does not adopt any chemical agents.

Decellularizing corneal tissue with detergent treatment is difficult, whereas by using HHP treatment, almost complete decellularization of corneal tissue was accomplished [15]. Experiments with decellularized porcine corneal tissue implanted into rabbit eye showed superior functionality, i.e. transparency. However, there are still few reports on decellularization using, and there is no a specific study on the decellularization condition yet.

In this study, we attempted to use HHP to prepare decellularized cardiovascular tissues. Cardiovascular tissues, such as heart valve, aortic vessel, and small diameter blood vessel, should have superior properties to corneal tissue. For instance, they should be pressure resistant, anti-thrombogenic, and have anti-calcification ability. Porcine aortic blood vessel was decellularized by HHP treatment and the efficiency of decellularization, mechanical properties, immunogenicity, and in vivo performance were evaluated. This

* Corresponding author. Division of Biofunctional Molecules, Institute of Biomaterials and Bioengineering, Tokyo Medical and Dental University, 2-3-10, Kanda-surugadai, Chiyoda-ku, Tokyo 101-0062, Japan. Fax: +81 3 5280 8028.
** Corresponding author. National Cardiovascular Center, 5-7-1, Fujishirodai, Suita, Osaka 565-8565, Japan. Fax: +81 6 6954 4746.
E-mail addresses: fujisato@bme.oit.ac.jp (T. Fujisato), kishida.fm@tmd.ac.jp (A. Kishida).

0142-9612/$ – see front matter © 2010 Elsevier Ltd. All rights reserved.
doi:10.1016/j.biomaterials.2010.01.073

article focuses particularly on the preparative conditions for the decellularized blood vessel using the HHP technique. Determining the optimal conditions for obtaining biologic scaffold with undamaged extracellular matrices (ECM) and high decellularization was one of the goals of this study. For this purpose, the effect of water state (ice formation) during pressurization was investigated in detail.

2. Materials and methods

2.1. Materials

Fresh porcine hearts were obtained from a local slaughterhouse (Tokyo Shibaura Organ Co. Ltd, Japan). The aortic blood vessel next to the aortic valves was excised and cut into 1 × 0.2 cm pieces. Aortic tissue was cleaned to remove fat and stored immediately at 4 °C in phosphate buffer saline (PBS) without Ca^{2+} or Mg^{2+} for transport to the laboratory for further processing.

2.2. Decellularization by HHP

2.2.1. Pressurization profile

The decellularization protocol consisted of two steps: 1) HHP treatment and 2) washing. The blood vessel samples were pressurized using a cold isostatic pressurization machine (Dr. Chef; Kobelco, Japan). The detailed procedures were as follows. After packing each sample in a plastic bag filled with PBS, the bag was immersed into the transmission fluid in the sample chamber of the machine. Before compression, the onset temperature was set at 10 or 30 °C. Then, the atmosphere inside the sample chamber was pressurized at a predetermined rate (196.1 or 65.3 MPa/min) until the pressure reached 980 MPa. The pressure was maintained at 980 MPa for 10 min and then was decreased at a predetermined rate (196.1 or 65.3 MPa/min) until atmospheric pressure was reached.

2.2.2. Washing process

After the HHP process, samples were washed with PBS for 14 days. Then, the samples were immersed in new PBS containing antibiotics and stored at 4 °C.

2.3. Preparation of decellularized aortic scaffold by detergent treatment

Triton® X-100 treatment: The blood vessels were placed in a solution of 1% Triton® X-100 (Sigma–Aldrich, Japan) with 0.02% EDTA (Wako, Japan) in PBS for 24 h, together with RNase A (20 mg/mL) (Roche, USA), DNase I (0.2 mg/mL) (Roche, USA), and 1% penicillin and streptomycin (Gibco, Japan) [16]. The blood vessels were washed with PBS several times to remove residual substances.

SDS treatment: The blood vessels were placed in a solution of 0.1% SDS (sodium dodecyl sulfate, Wako, Japan), together with RNase A (20 mg/mL), DNase (0.2 mg/mL), and 1% penicillin and streptomycin for 1 h at room temperature [17]. Then, they were washed with PBS for 48 h to remove residual substances.

Trypsin treatment: The blood vessels were placed in a trypsin solution (0.05% trypsin (Biochrom KG, Germany) and 0.02% EDTA) for 48 h at 37 °C [18].

2.4. Evaluation of decellularized tissue

2.4.1. Observation of structure of the decellularized tissue

Decellularized blood vessels were fixed by immersion with 10% neutral buffered formalin solution. The specimens were dehydrated in graded alcohol, embedded in paraffin blocks, and sectioned. The sections were stained with 1% hematoxylin–eosin (H–E). The slides were observed by optical microscope (Coolscope, Nikon Co., Ltd. Japan). For transmission electron microscopy (TEM), the decellularized blood vessels were fixed with 2.5% glutaraldehide in PBS. The specimens were prepared and observed by standard procedures for TEM.

2.4.2. Mechanical properties

Mechanical strength testing of the non-treated and the decellularized blood vessels was performed longitudinally. The samples were cut into dumbbell-shaped pieces. The tested parts were 15–20 mm long and 2 mm wide. Wall thickness was measured by micrometer prior to mechanical testing. Stress–strain curves were obtained with a creep meter RE2-33005 B (Yamaden Co., Ltd. Japan). Each sample was strained at a rate of 10 mm/min. All testing was conducted in air at room temperature (25 °C).

The stress–strain curve for each individual specimen was analyzed with regard to four parameters: early phase modulus of elasticity, late phase modulus of elasticity, ultimate tensile strength (UTS), and failure strain [19]. These parameters are defined that illustrates the typical stress–strain curve of blood vessel tissue. The analysis parameters from each group were averaged over the number of specimens in each group ($n = 10$). Results were expressed as the mean ± standard deviation (SD). Additionally, the individual means from each treatment group were compared by Student's t-test.

2.4.3. Quantification of residual DNA

Twenty-five mg of samples were placed in 10% proteinase K (Quiagen, USA) in lysis buffer solution overnight. The DNA from each sample was purified using a DNeasy® assay kit (Quiagen, USA). The DNA amounts were measured by spectrophotometry ($\lambda = 280$ nm).

2.4.4. Xeno-transplantation (pig to rat)

The animal study was performed in accordance with the NIH guidelines for the care and use of laboratory animals (NIH Publication 85-23, revised 1985) and the institutional guidelines for the care and use of experimental animals of Tokyo Medical and Dental University. Porcine blood vessel samples were dissected to be 1 × 1 cm segments. Native aorta samples and samples decellularized by several pressurization programs (the two experimental conditions) were implanted in the subcutaneous mucosal position of Wister rats (250 g, 7 weeks old) ($n = 3$). The implantation periods were 1 and 4 weeks. At a predetermined time, all animals were terminated by elective euthanasia with anesthesia of ether. The explanted specimens were fixed, dissected, and stained by H–E.

2.4.5. Measurement of immune response in xeno-transplantation area

The measurement of immune response was done by calculation of the area that was had an inflammatory response. Image J (National Institute of Health, USA) was used to measure the immunologic site surrounding in the transplant tissue.

2.4.6. Allo-transplantation (pig to pig)

The decellularized blood vessel was implanted into abdominal porcine aorta. No anticoagulants were administered after surgery. The implantation periods were 4, 12, and 24 weeks. The explanted specimens were fixed, dissected and stained by H–E.

3. Results and discussion

3.1. Effect of ice formation during pressurization

The effect of high pressure on the extracellular matrix is largely still unknown. Denaturation of proteins at high pressure has been widely studied [20,21] while the research on collagen is quite limited. In our HHP treatment, collagen denaturation would have a great impact on the physical properties of the tissue. So, an important point in this study was to find out whether the extracellular matrix structure was maintained throughout the treatment.

First, the relationship between the pressure and the temperature of the treatment chamber was studied. Pressure–temperature curves for each pressurization condition were drawn in the phase diagram of water to see whether ice would form during the pressurization and depressurization processes. It is known that the lowest freezing point of water is −20 °C at about 200 MPa, and it increases to 30 °C at 980 MPa (The phase diagram of water is shown in Fig. 1, inset) [22,23]. The phase diagram of the pressure–temperature graph for water suggests that increased pressure would induce the water to freeze. This suggests that the high pressure treatment of native tissue may also cause the formation of ice during our process. It has been reported that the freezing process generally destroys the structure of biological tissues under normal pressure [24,25]. Therefore, temperature control during pressurization is necessary.

As shown in Fig. 1 (large image), under condition I (the starting temperature was 10 °C, pressurization and depressurization rates were 196.1 MPa/min), the samples passed the freezing zone from 937 to 980 MPa during the increasing pressure process. In our conditions, the highest pressure was maintained for 10 min before depressurization. From 980 to 759 MPa, the water would be in the freezing state and would return to the liquid state after further depressurization under 759 MPa. On the other hand, under condition II (the starting temperature was 30 °C, pressurization and depressurization rates were 65.3 MPa/min), the samples did not pass the freezing zone throughout the pressurizing process. This means that the destruction of tissue structure by the formation of ice would not occur when the starting temperature was 30 °C. It should be noted that the pressurization and depressurization rates should be controlled to maintain the starting temperature. Fast